# The COLA Atmosphere-Biosphere General Circulation Model
# Volume 1: Formulation

James L. Kinter III
David DeWitt
Paul A. Dirmeyer
Michael J. Fennessy
Ben P. Kirtman
Larry Marx
Edwin K. Schneider
J. Shukla
David M. Straus

*Center for Ocean-Land-Atmosphere Studies*
*Institute of Global Environment and Society, Inc.*
*4041 Powder Mill Road, Suite 302, Calverton, MD 20705.*

October 1997

## Preface

This report documents the current version (1.12) of the Center for Ocean-Land-Atmosphere Studies atmospheric general circulation and land surface biosphere model is documented. The governing equations for atmospheric motion and thermodynamics as well as descriptions of the full set of subgrid scale physical parameterizations are provided.

The model is suitable for global climate studies on monthly, seasonal and interannual time scales. A large body of scientific research has been conducted with this model, and it is currently in use worldwide for both research and operational forecasting of the Earth's atmosphere. A companion report will be released soon that provides information on how to use the model.

Since the model evolves as more is learned about its behavior and its fidelity to the observations of the Earth's atmosphere, this report is merely a "snapshot" of the current state of the model. We are distributing this report in both print and electronic form so that documentation of future revisions of the model can be rapidly disseminated via the World Wide Web. Please see the following URL for the latest version of this document:

http://grads.iges.org/agcm/

## Table of Contents

## Introduction

The basic tool for meteorological research at the Center for Ocean-Land-Atmosphere Studies (COLA) is a general circulation model (GCM) of the Earth's atmosphere that includes a detailed model of the land surface. The COLA GCM has evolved over several years. The initial realization of the model was the GCM being used in 1985 for medium range numerical weather prediction at the National Meteorological Center (NMC; recently reorganized as the National Centers for Environmental Prediction - NCEP) that was graciously provided to COLA. The model currently used for global medium range forecasting (MRF) as well as for retrospective data analysis (reanalysis) by NCEP (Kanamitsu, 1989; Kanamitsu et. al., 1990) is also a descendent of the 1985 NMC model. The 1985 NMC model was an amalgam of the global spectral dynamics code developed at NMC (Sela 1980) and the subgrid scale physical parameterizations developed at the Geophysical Fluid Dynamics Laboratory (GFDL) of NOAA at Princeton University (Miyakoda and Sirutis, 1977). We adapted the MRF by adding a number of diagnostic calculations in order to promote better understanding of the physical processes being simulated and their relative importance. Computer code was also added to make it possible to integrate the model for more than 10 simulated days, and the capability to apply observed boundary conditions was implemented. Seasonal simulations made with the enhanced model were reported by Kinter et al. (1988). The model computer code has been adapted to a number of computing environments including the Control Data Cyber 205, the Cray X-MP, Y-MP, J90 and C90 systems, and several Unix workstation platforms.

Both COLA and NCEP have changed the original model since 1985 in several significant ways. As both versions of the model evolved, it became clear that the changes being effected by NCEP to improve the medium range forecast were made more frequently than was optimal for a stable climate model. Likewise, the experimental nature of the changes made by COLA made it impractical for the NCEP to adopt those changes operationally. As a result, the models have diverged, so that they are now substantially different from one another. There are major differences in the treatment of nearly all the subgrid scale physical parameterizations and, more recently, the hydrodynamics. There is also a difference in the horizontal and vertical resolution of the two models.

This document is intended as an overview of the COLA GCM. It consists of two volumes: the first volume describes the formulation of the dynamics and physical parameterizations, and the second functions as a user guide. The documentation of the NCEP MRF (NMC Development Division Staff, 1988; hereinafter referred to as MRF88) is referenced in places where the two models are similar. Where they are significantly different, this document describes the COLA formulation. The current NCEP formulation, including updates to MRF88, is described in Kanamitsu (1989) and Kanamitsu et al. (1990).

The COLA GCM is coded so that many of the FORTRAN parameter settings may be changed. These include the horizontal and vertical resolutions, switches to include or exclude various parameterization schemes, and some flexibility in the diagnostic variables that are calculated and saved. A large number of simulations with the current version of the COLA GCM have been made with three horizontal resolutions: R15, T30 and R40. The horizontal resolution designator has a letter denoting the shape of spectral truncation (see section IB) and a number referring to the largest wave number resolved. The "R" refers to the rhomboidal truncation and "T" is for

triangular truncation. Various vertical resolutions, including five, nine and 18 levels, have been used for climate simulation. The model atmospheric variables are predicted at all vertical levels.

This volume is divided into chapters that describe individual major processes in the GCM. The first chapter reviews the equations of motion and the laws governing the conservation of mass and thermodynamics. In chapter II, the radiative transfer parameterization is described. The remaining chapters describe the sub-grid scale parameterizations. In chapter III, the surface layer physics is described. Planetary boundary layer processes are discussed in chapter IV. Chapter V is a discussion of all moist physical processes including the various ways in which water phase changes are simulated. The initial conditions and boundary conditions are described in chapters VI and VII, respectively.

## I. Hydrodynamics

### A. Equations of motion

The basic physical laws that govern atmospheric motions in the COLA GCM are the conservation laws for mass (dry air and moisture conserved separately), energy, and angular momentum expressed in the spherical shell geometry and rotating frame of reference of the Earth's atmosphere. The equations that are employed include the equations of motion, continuity equations for dry air and water vapor, and the first law of thermodynamics. The equation for the vertical component of velocity (parallel to the gravitational force vector) is replaced by a diagnostic relationship on the assumption that, on the spatial and temporal scales of interest, motions are in hydrostatic balance. The complete set of equations which describe such a fluid system are termed the primitive equations. The model is global in extent and conforms to a spherical shell geometry whose vertical extent is sufficiently small that the distance from the center of the Earth may be assumed to be approximately constant (equal to the radius of the Earth). The distance above the surface of the Earth is included as an independent variable.

Because the atmosphere is assumed to be in hydrostatic balance, it is convenient to express the vertical variation in the primitive equations in terms of a pressure coordinate. In practice, as recommended by Phillips (1957), the vertical coordinate is pressure, $p$, normalized by its value at the surface, $p_S$:

$$\sigma = \frac{p}{p_s} \qquad (1)$$

so that the vertical coordinate, $\sigma$, varies from a value of 1 at the Earth's surface to a value of 0 where the atmospheric pressure effectively vanishes. We write the conservation of angular momentum as follows:

$$\frac{d\vec{V}}{dt} = - RT\,\vec{\nabla} ln\, p_s - \vec{\nabla}\Phi - f\,\hat{k}x\vec{V} + \vec{F} \qquad (2)$$

where $V$ is the horizontal wind vector, $R$ is the dry air gas constant, $T$ is the temperature, $\Phi$ is the geopotential, $f$ is the Coriolis parameter, $k$ is the unit vector in the vertical direction, and $F$ is the vector sum of all frictional forces. This equation indicates that the acceleration of horizontal atmospheric motion results from the sum of the pressure gradient force, the Coriolis force due to the rotating frame of reference, and the sum of all frictional forces. By applying vector identities and the curl and divergence operators to this equation, we obtain the scalar vorticity and divergence equations:

$$\frac{\partial \eta}{\partial t} = -\frac{1}{a\cos^2\phi}\left(\frac{\partial A}{\partial \lambda} + \cos\phi \frac{\partial B}{\partial \phi}\right) \qquad (3)$$

$$\frac{\partial D}{\partial t} = \frac{1}{a\cos^2\phi}\left(\frac{\partial B}{\partial \lambda} - \cos\phi \frac{\partial A}{\partial \phi}\right) - \nabla^2 (E + \Phi + RT_0 \ln p_s) \qquad (4)$$

where $\eta$ is the absolute vorticity ($\eta=\zeta+f$, where $\zeta$ is the relative vorticity), $a$ is the Earth's radius, $\phi$ is the latitude, $\lambda$ is the longitude, $T_0$ is the global mean temperature and $A$, $B$ and $E$ are defined as follows:

$$A = \eta U + \frac{RT'\cos\phi}{a}\frac{\partial \ln p_s}{\partial \lambda} + \dot{\sigma}\frac{\partial V}{\partial \sigma} - F_\phi \cos\phi \qquad (5)$$

$$B = \eta V - \frac{RT'}{a}\frac{\partial \ln p_s}{\partial \lambda} - \dot{\sigma}\frac{\partial U}{\partial \sigma} + F_\lambda \cos\phi \qquad (\dot{\sigma} = \text{vertical velocity}) \qquad (6)$$

$$E = \frac{\vec{V}\cdot\vec{V}}{2} \qquad (7)$$

where $U = u \cos\phi$, $V = v \cos\phi$, $u$ and $v$ are the components of the horizontal wind vector in the longitudinal and latitudinal directions, respectively, $T'$ is the deviation of temperature from its global mean $T_0$, $F_\lambda$ and $F_\phi$ are the components of the friction force in the longitudinal and latitudinal directions, respectively, and $E$ is the kinetic energy.

The first law of thermodynamics is written

$$\frac{d\ln\theta}{dt} = \frac{\dot{Q}}{c_p T} \qquad (8)$$

where $\theta$ is the potential temperature ($\theta = T(p/p_0)^\kappa$ where $p_0$ is a standard pressure and $\kappa = R/c_p$), $Q$ is the heating rate, and $c_p$ is the specific heat of air at constant pressure. By expanding the total derivative and rearranging terms, we can write the first law as:

$$\frac{\partial T}{\partial t} = -\vec{V}\cdot\vec{\nabla}T + \kappa T\left(\frac{\partial}{\partial t} + \vec{V}\cdot\vec{\nabla}\right)ln\, p_s + \frac{\dot{Q}}{c_p} - T\left(\kappa + \frac{\partial}{\partial\sigma}\right)\dot{\sigma} - \frac{\partial}{\partial\sigma}(\dot{\sigma}T) \qquad (9)$$

a form that is more suitable for vertical differencing (see below).

The mass conservation law is expressed mathematically as the continuity equation. This equation may be vertically integrated to obtain an equation for the evolution of the surface pressure:

$$\frac{\partial ln\, p_s}{\partial t} + \int_0^1 \left(\vec{V}\cdot\vec{\nabla}\ln p_s + \vec{\nabla}\cdot\vec{V}\right)d\sigma = 0 \qquad (10)$$

Note that the upper and lower boundary conditions of no flow normal to the ground or through the "top" of the atmosphere have been applied. Likewise, a conservation equation may be expressed for water vapor in the atmosphere given a set of sources and sinks (represented by $S$):

$$\frac{dq}{dt} = S \qquad (11)$$

where $q$ is the specific humidity.

The equations (3), (4), (9), (10) and (11) are the continuous form of the equations used to predict vorticity, divergence, temperature, surface pressure and atmospheric water vapor in the GCM. The geopotential that is needed in the divergence equation is obtained from vertical integration of the hydrostatic equation:

$$\frac{d\Phi}{dln\sigma} = -RT \qquad (12)$$

and, similarly, the vertical velocity is diagnosed by vertical integration of the divergence from the surface to the level in question:

$$\dot{\sigma} = -\frac{\partial \ln p_s}{\partial t} - \int_0^{\sigma}\left\{\vec{V}\cdot\vec{\nabla}\ln p_s - \vec{\nabla}\cdot\vec{V}\right\}d\sigma' \qquad (13)$$

While many texts provide derivations of these equations in a spherical shell geometry, the most relevant reference for the equations used in the COLA model is Sela (1980) or, alternatively, MRF88 (chapter 2). In addition to the above prognostic variables, the model also diagnoses clouds in four categories at all levels (see section IIC), sea ice temperature, and the land surface variables used in the biosphere model, namely, deep soil temperature, ground surface temperature, canopy temperature, three stores of soil moisture, ground water storage (ponding) and canopy water storage (either liquid or solid, i.e., snow) are also predicted (see section IIIB).

B. Model discretization

The equations described above are solved numerically. In order to place the equations in a form suitable for numerical solution, the four independent dimensions of the problem must be expressed in discrete coordinates. The time dimension is divided into evenly spaced time steps and differencing is carried out by means of a semi-implicit scheme described below. Variations in the horizontal dimensions are represented as coefficients of projection onto an orthonormal set of basis functions that are particularly appropriate for fluid motions in a spherical geometry, namely, the spherical harmonics.

The spherical harmonics are the eigenfunctions of the spherical form of Laplace's equation that governs tidal motions. Because the atmosphere is well stratified and motions are assumed hydrostatic, the surface spherical harmonics are used instead of the full three dimensional spherical harmonics. This affords analytic evaluation of derivatives in the horizontal directions. The application of this technique to atmospheric motion was suggested by Platzman (1960) and made practical for reasonable resolutions by means of the spectral transform method (Orszag, 1970). The spherical harmonics may be written as the product of Fourier components and associated Legendre functions. The Fourier components $(e^{im\lambda})$ represent variations in the longitudinal direction, being a natural choice given the periodic nature of the spherical shell geometry in this direction. Variations in the latitudinal direction are represented by the associated Legendre polynomials $(P_m^n)$ expressed as functions of the sine of latitude. Because the associated Legendre polynomials satisfy the geometrically determined boundary conditions at the poles and because they satisfy Laplace's equation governing tidal motions on the sphere they are a natural choice for representing latitudinal variations. The spherical harmonic of order $m$ and degree $n$ is the product of $(P_m^n)$ and $(e^{im\lambda})$. Any piecewise continuous scalar field on the surface of a sphere may be represented as a series of these orthogonal spherical harmonics. In practice, the series is truncated at a given two-dimensional wave number, with higher order terms in the series being ignored.

The spherical harmonics which are retained in the truncated series may be represented in a two dimensional $(m,n)$ wave number space, where $m$ is the zonal wave number and $n$-$m$ is the number of zeroes of $P_m^n$, and the truncation may have various shapes. The two most commonly used truncations are triangular in which the sum of the zonal and latitudinal limits of truncation is a constant and rhomboidal in which the two truncation limits are the same. The triangular truncation has the advantage that all basis functions having the same scale are either included or dropped. The rhomboidal truncation was the first one adopted for numerical treatment of the primitive equations because it was easier to code for optimal performance on fast vector supercomputers (Bourke, 1972).

The spectral method of solution, in which prognostic variables are expressed in series of orthogonal basis functions, has the drawback that nonlinear terms in the equations involve quadratic and triple products (and therefore integrals of quadratic and triple products) which require a great deal of computation which exceeds available computer resources at high model resolution. Orszag (1970) suggested a method for making this computation feasible. By representing the quadratic terms on a grid to which the prognostic variables have already been transformed, the contributions of these terms to the time tendencies could be computed using the back transform. By using suitable numerical algorithms to gain computational efficiency (fast Fourier transform) and retain the exactitude of the spectral treatment (e.g. by using Gaussian quadrature in the integral with respect to latitude), it was shown that the spectral transform method is computationally superior to the direct spectral method (Orszag, 1970; Bourke, 1972). The grid on which the most computationally efficient transform may be effected is called the Gaussian grid to recall the form of quadrature that is employed. A more complete and rigorous development of spherical harmonics, the spectral method and the spectral transform method may be found in Haltiner and Williams (1980).

The elevation of the Earth's surface is represented by interpolating the Navy 10' by 10' observed topography to the model Gaussian grid, iteratively filtering and transforming the result to its spectral representation (Fennessy et al., 1994).

Vertical derivatives are evaluated by finite differencing in $\sigma$. The vertical differencing is written in an energy conserving form (Arakawa, 1972). Terms involving derivatives with respect to $\sigma$ are expressed in flux form, e.g.,

$$\dot{\sigma}\frac{\partial q}{\partial \sigma} = \frac{\partial \dot{\sigma} q}{\partial \sigma} - q\frac{\partial \dot{\sigma}}{\partial \sigma} \qquad (14)$$

The first term may then be approximated as:

$$\frac{\partial \dot{\sigma} q}{\partial \sigma} = \frac{1}{\Delta \sigma}(\dot{\sigma}_{k+1}\hat{q}_{k+1} - \dot{\sigma}_k \hat{q}_k) \qquad (15)$$

where the subscript $k$ refers to the $k^{th}$ vertical (discrete) level. The hat is a vertical averaging operator:

$$\hat{q}_{k+1} = \frac{1}{2}(q_{k+1} + q_k) \qquad (16)$$

As a result, terms involving vertical derivatives in equations (3), (4), (9), (10) and (11) may be expressed in finite difference form by analogy with the above. The thermodynamic equation is rearranged for energy conservation as follows:

$$\frac{\partial T_k}{\partial t} = -\frac{\vec{V}k}{\cos\varphi}\cdot\vec{\nabla}T_k + \kappa T_k\left(\frac{\partial}{\partial t} + \frac{\vec{V}_k}{\cos\varphi}\cdot\vec{\nabla}\right)ln\, p_s + \dot{Q}/c_p \qquad (17)$$

$$-\frac{1}{2\Delta_k}\left[\dot{\sigma}_{k-1}\left(\frac{\Pi_k}{\Pi_{k+1}}T_{k+1} - T_k\right) + \dot{\sigma}_k\left(T_k - \frac{\Pi_k}{\Pi_{k+1}}\right)\right] \qquad (18)$$

$$\text{where}\quad \Pi_k = \left(\frac{p_k}{p_o}\right)^{\kappa}$$

$$\text{and}\quad \Delta_k = \sigma_{k+1} - \sigma_k$$

The arrangement of variables on the discrete vertical levels is shown in Fig. 1. A full derivation of the vertical finite difference equations is given in MRF88 (chapter 2).

Spectral truncation of the prognostic mass variable, log of surface pressure, results in non-conservation of atmospheric mass. In the COLA GCM, the surface pressure is adjusted uniformly over the globe at periodic simulated intervals (typically one month) to ensure that the total mass of the atmosphere remains constant. The spectral truncation of specific humidity results in negative values of this variable, under certain circumstances. A scheme (ECMWF, 1988) in which moisture is borrowed from lower atmospheric layers is employed to restore negative values of specific humidity to zero. Both conservation restoration schemes are described in greater detail in Schneider and Kinter (1994).

The time domain of the model is expressed in discrete steps of a fixed length. Given a set of initial conditions for the model prognostic variables, their time evolution is computed by "marching" forward using the time derivatives (as expressed in equations 1 - 5). Since the equations describe fluid flow which supports wave motions, the size of the time step is constrained by the speed of the fastest such wave due to the Courant-Friedrichs-Levy (CFL) computational instability associated with aliasing that wave (e.g. Haltiner and Williams, 1980). Due to the presence of fast gravity waves in the atmosphere, this constraint can result in an extremely small time step that is prohibitive in terms of computational speed, so some means of overcoming this limitation needs to be employed. In many GCMs, the method of choice is to treat the terms in the equations associated with gravity waves separately from the other terms. In particular, the pressure gradient term in the momentum equation (or its analog in the vorticity and divergence equations) and the divergence term in the surface pressure tendency equation are stepped forward in time implicitly while the other terms are treated explicitly (e.g., leap frog scheme). An implicit time differencing scheme is one in which the value of a variable at a future time appears on the right hand side of the equation, so that a system of simultaneous equations (whose order is the number of spatial degrees of freedom) must be solved at each time step. Its

advantage is that it is unconditionally stable (no computational instability), so that the time step can be arbitrarily large. Its disadvantages are the huge computational expense of inverting a matrix at each time step and the phase error introduced by the differencing scheme which grows with the size of the time step (Haltiner and Williams, 1980). Thus, a balance must be struck between computational efficiency and numerical accuracy. A scheme in which part of the equation is treated implicitly is called semi-implicit. The COLA model uses such a semi-implicit scheme for the divergence, continuity and hydrostatic equations. A full derivation of the semi-implicit divergence, temperature, and moisture equations is given in MRF88 (chapter 2).

A drawback of the explicit leap frog scheme used to march the vorticity and moisture equations is the tendency for the solution to diverge at alternative time steps. To suppress the time splitting, a Robert (1969) time filter is employed.

C. Horizontal diffusion

Horizontal diffusion is necessary to control small scale "noise" which would otherwise arise in the model. The origins of the noise include (i) the effects of a finite spectral truncation, which interrupt the downscale cascade of energy, (ii) small scale gravity waves caused by the sub-grid scale physical processes, and (iii) other, purely computational effects. Since the larger, well resolved scales should not be affected, a scale selective biharmonic type diffusion is utilized. Experience at NCEP has shown that for the variables of moisture and temperature, this diffusion must be along pressure surfaces and not along the model $\sigma$ surfaces, for otherwise excessive precipitation in regions of steep terrain results (MRF88). For vorticity and divergence, diffusion along $\sigma$ surfaces seems to be adequate.

The relationship between a horizontal derivative on constant pressure surfaces of any variable $\Psi$ and the corresponding derivative on constant $\sigma$ surfaces is:

$$\left[\frac{\partial \Psi}{\partial x}\right]_p = \left[\frac{\partial \Psi}{\partial x}\right]_\sigma + \left[\frac{\partial \Psi}{\partial ln\sigma}\right]\left[\frac{\partial \pi}{\partial x}\right] \qquad (19)$$

where $\pi$ is the log of surface pressure, $x$ is one of the horizontal directions, and $\Psi$ is an arbitrary scalar field. The subscripts $p$ and $\sigma$ refer to derivatives along constant pressure and $\sigma$ surfaces, respectively. Applying (19) twice in both horizontal directions, we obtain:

$$\nabla^2_p \Psi = \nabla^2_\sigma \Psi\, 2\nabla\pi\nabla - \nabla_\sigma\left[\frac{\partial \Psi}{\partial ln\sigma}\right]\left[\frac{\partial \Psi}{\partial ln\sigma}\right]\nabla^2_\sigma \pi + \left[\frac{\partial^2 \Psi}{\partial (ln\sigma)^2}\right]|\nabla\pi|^2 \qquad (20)$$

Experiments have shown that an adequate (and computationally efficient) approximation to the full equation (20) is given by retaining only the first and third terms on the right hand side of (20), and by replacing $\Psi$ with its horizontal average (denoted by an overbar) in the third term. Expressing $\Psi$ in spectral form, the $(m,n)$ component of the diffusion along pressure surfaces may be written:

$$(\nabla^2_p \Psi)^m_n = \frac{n(n+1)}{a^2} \Psi^m_n + \frac{\partial \overline{\Psi}}{\partial(ln\sigma)} \pi^m_n \qquad (21)$$

where $a$ is the radius of the Earth. Applying (21) twice, and again assuming constant vertical derivatives, we obtain:

$$(\nabla^4_p \Psi)^m_n = \frac{n^2(n+1)^2}{a^4} \Psi^m_n + \frac{\partial \overline{\Psi}}{\partial(ln\sigma)} \pi^m_n \qquad (22)$$

The above formulation (22) is used for temperature and moisture. For vorticity and divergence, the vertical derivative term embodying the corrections to ensure diffusion along a constant pressure surface is omitted.

The diffusion coefficient is set to a value that causes the highest resolved total wavenumber component to damp to $1/e$ of its initial value in $T$ hours in the absence of all other processes. For divergence, the value of $T$ is set to 21 hours, and for temperature, vorticity and moisture, the corresponding time is 28 hours.

## II. Radiation

A. Short wave (solar) heating

The driving force behind all atmospheric motions relative to the Earth's surface is the differential latitudinal heating due to absorption of radiation from the sun. The sun's emission spectrum peaks in the visible band at the relatively short wavelength end of the electromagnetic spectrum and is therefore termed short wave radiation. Because the sun's rays are not vertical at all latitudes, there is a strong variation in solar heating over the globe. The presence of clouds in the atmosphere also strongly modulates the absorption of solar radiation. Clouds scatter short wave radiation as well, and, as such, are responsible for a substantial fraction of the planetary albedo in regions that are not covered by ice.

The short wave radiation formulation is that of Lacis and Hansen (1974) as modified by Davies (1982). It includes atmospheric heating due to the absorption of solar radiation by water vapor and ozone. The ozone concentration is specified (rather than predicted) from a zonal mean climatology described in section VII (C). Since cloudiness has a major impact upon the amount of solar radiation that is scattered and absorbed, the predicted cloudiness is used in the calculation of short wave radiation. In typical climate simulations, the short wave heating is calculated each hour of simulated time. The short wave heating is temporally smoothed by linearly interpolation between calculations to the current time step.

B. Long wave heating

Balancing the absorption of solar radiation, the Earth emits radiation to space resulting in a conservation of energy for the Earth/atmosphere system in the time and global mean. The terrestrial radiation to space, which peaks in the infrared band is called outgoing long wave radiation. Long wave emission from the Earth's surface may be absorbed by constituents in the atmosphere, and it may be re-emitted as well. The distribution of surface emissions as well as absorbing and emitting species and clouds is not uniform over the globe, so the long wave heating is not equally distributed. The unequal distribution of short wave and long wave heating induces pressure gradients that give rise to atmospheric motions.

The long wave heating is a broad band parameterization formulated for fast computation by Harshvardhan et al. (1987). It includes atmospheric heating due to the absorption of terrestrial radiation by water vapor (predicted), carbon dioxide (specified), and clouds (predicted), as well as other less important species. The water vapor mixing ratio is computed from the specific humidity and virtual temperature that are carried as prognostic variables in the model equations. The cloud amount is predicted according to the scheme described in section II (C). The species that are radiatively active in the terrestrial wavelength band are described in section VII (C). In typical climate simulations, the long wave heating is computed at least every three hours of simulated time in order to adequately resolve the diurnal cycle of terrestrial radiation.

C. Cloud radiation interaction

As described above, the short wave and long wave heating parameterizations are substantially affected by the presence of clouds. Formerly, the COLA GCM included specified clouds from a zonal mean GFDL cloud climatology (Kinter et al., 1988), but this approach has been supplanted in most GCMs by predicted clouds. Our motivation is that predicted clouds alter the energy balance and may provide a considerably greater reservoir of available potential energy to drive atmospheric motions than the zonally symmetric clouds (Hou, 1990). As such, predicted clouds are employed in the model using a scheme that is a hybrid of the scheme implemented by Hou (1990) and the scheme employed in the National Center for Atmospheric Research (NCAR) Community Climate Model (CCM2; Kiehl et al., 1994). Hou's scheme is further described by DeWitt (1996) and is based on the work of Slingo (1987). Following is a brief summary of the Hou (1990) scheme and a description of how it was changed to include beneficial features of the NCAR CCM2 scheme.

In the COLA GCM, clouds are divided into supersaturation and convective types (sections V - A and V - B). Supersaturation clouds are further divided according to the pressure level at which the cloud occurs. Supersaturation clouds are classified as low clouds if they occur between a pressure of 1000 and 700 millibars; middle clouds if they occur between a pressure of 700 and 400 millibars; and high clouds if they occur above 400 millibars. Formation of the supersaturation clouds is according to the equation:

$$C_k = \left( \frac{RH_k - RH_c}{1 - RH_c} \right)^2 \qquad (23)$$

where $C_k$ is the fractional cloud cover which is bounded by 0 and 1, $RH_k$ is the relative humidity within layer $k$, and $RH_c$ is the critical relative humidity which is a function of cloud type (Smagorinsky, 1960). The values of $RH_c$ are 0.8 for low and middle clouds and 0.9 for high clouds. If the relative humidity within a layer is less than the critical relative humidity for that layer then no supersaturation cloud will form. The low clouds are further modified by the vertical velocity of the layer in which they occur. The modification of the low supersaturated clouds due to vertical velocity is according to:

$$CLF = C_k \begin{bmatrix} 0 & \omega > 5x10^{-5} \\ 1 - m^2 & -5x10^{-5} \le \omega \le 5x10^{-5} \\ 1 & \omega < -5x10^{-5} \end{bmatrix} \qquad (24)$$

$$where\ m = (\omega + 5x10^{-5})\ x\ 10^4$$

and $\omega$ is the vertical pressure velocity in centibars per second.

In addition to the formation of low clouds by the above formula, low clouds are also allowed to form if a temperature inversion of sufficient strength is diagnosed. The formation of the

inversion cloud is further modified by the relative humidity at the base of the inversion. The inversion clouds form according to the formula:

$$C_{inv} = 6.67\left(\frac{d\theta}{dp} - \frac{d\,\theta_c}{dp}\right) RHF \;\; for \;\; \frac{d\theta}{dp} < \frac{d\,\theta_c}{dp} \qquad (25)$$

where

$$RHF = \begin{bmatrix} 0.0 & RH_b < 0.6 \\ 1.0 - \dfrac{(0.8 - RH_b)}{0.2} & 0.6 \le RH_b \le 0.8 \\ 1.0 & RH_b > 0.8 \end{bmatrix}$$

where $RH_b$ is the relative humidity at the inversion base and $d\theta_c/dp$ is the critical lapse rate which is used to determine the presence of an inversion. When low clouds form, they are prescribed to be two layers thick since the lower layers in the GCM are quite thin. If more than one layer within the same supersaturation cloud domain (i.e. low, middle, high) has a prescribed cloud amount, only the layer with the highest cloud amount is kept for that domain. For the purposes of computing the radiative effect of clouds, all clouds are treated as randomly overlapping.

Convective cloud is diagnosed according to the three hour mean precipitation rate using the formula:

$$C_c = a + b\ln P \qquad (26)$$

where $a$ and $b$ are prescribed constants as in Slingo (1987) and $P$ is the cumulative mean convective precipitation rate in units of mm day$^{-1}$. This cloud amount is assigned to every layer in between the base and top of the diagnosed convection. The convective cloud fraction is constrained to be smaller than 0.8. If the convective cloud fraction is diagnosed to be greater than 0.4 for some time step and the convection extends above 400 millibars, then an anvil cloud is diagnosed at the top level of convection according to the formula:

$$C_{anvil} = 2.0\ (C_c - 0.3) \qquad (27)$$

The prescription of the optical properties of the clouds follows Harshvardhan et al. (1989). The approximation of cloud pressure optical thickness in the short wave spectrum is according to:

$$\tau_{sw} = \begin{bmatrix} 0.025\Delta p_c & T_c \le -20 \\ 0.05\Delta p_c & -20 \le T_c \end{bmatrix} \qquad (28)$$

The variable $T_c$ in this formula is the mean cloud temperature (in °C) and $\Delta p_c$ is the pressure thickness of the cloud (in hPa). The formula for long wave cloud emissivity is specified as:

$$\varepsilon = 1 - \exp(-\beta \Delta p_c) \qquad (29)$$

$$where \quad \begin{Bmatrix} \beta = 0.01 & for \;\; Tc \le -20 \\ \beta = 0.05 & for \;\; -20 \le Tc \end{Bmatrix}$$

The Hou (1990) formulation, especially in the short wave band, was found by DeWitt and Schneider (1996) to be at variance with the top of the atmosphere fluxes observed in the Earth Radiation Budget Experiment (ERBE; Barkstrom, 1984; Barkstrom et al., 1989; data set documented by Hurrell and Campbell, 1992). DeWitt and Schneider (1996) implemented a revised formulation of cloud radiation interaction that incorporated some of the favorable aspects of the NCAR CCM2 cloud scheme. One important aspect of the resulting hybrid scheme is that convective cloud amount is first determined for the entire depth of the cloud, and then the amount at each model level within the cloud is determined as a function of the total. The total convective cloud amount is specified as

$$C_{cont} = 0.20 + 0.038P \quad \text{for } P > 0 \text{ and } C_{cont} \le 0.8 \qquad (30)$$

The total convective cloud amount $C_{cont}$ is, as in Hou (1990), constrained to be less than 0.8. In each layer between the cloud base and cloud top, the convective cloud amount is defined as $C_{con} = 1 - (1 - C_{cont})^{1/N}$ where N is the number of layers between the convective cloud base and top. If the cloud top occurs above the 400 mb level, then an anvil cloud associated with the deep convection is assigned to the level above the cloud top. The anvil fraction is set to $C_{anvil} = 2\, C_{cont}$. In addition to the clouds associated with deep convection, shallow convective clouds are diagnosed if the model's shallow convection scheme is invoked. The total amount of shallow convective cloud is set to 0.3 and the cloud amount assigned to each layer between the shallow convective cloud base and cloud top is $1 - 0.7^{1/M}$ where M is the number of such layers.

In contrast to the Hou (1990) scheme, supersaturation clouds are assigned a cloud fraction as:

$$C_{rh} = \left( \frac{RH - 0.9}{0.1} \right)^2 \qquad (31)$$

where RH is relative humidity. The low level inversion clouds are diagnosed using:

$$C_{inv} = -6.67\left(\frac{d\theta}{dp} - \frac{d\theta_c}{dp}\right)RHF \qquad (32)$$

where $d\theta/dp$ is the lapse rate of potential temperature and $d\theta_c/dp$ is the critical value of the lapse rate that must be exceeded in order for inversion clouds to be diagnosed. RHF is the relative humidity function defined above, as in Hou (1990).

The total cloud fraction in any layer is defined as

$$C_{tot} = (1.0 - C_{conh})\, C_{ls} + C_{conh} \qquad (33)$$

where

$$C_{conh} = C_{con} + C_{shal} + C_{anvil} \qquad (34)$$

and

$$C_{ls} = C_{rh} + C_{inv}. \qquad (35)$$

## III. Surface Layer Processes

The atmosphere and the Earth's surface, whether land or ocean, exchange momentum, heat and moisture through a variety of processes. The exchange takes place in a relatively thin layer of the atmosphere called the surface layer (distinct portion of the planetary boundary layer - see section IV - nearest the Earth's surface). The COLA GCM employs an empirical relation that approximates Monin-Obukhov similarity theory to determine the transfer or drag coefficients. The empirical relations are different for ocean and land surfaces.

A. Oceans

Latent and sensible heat fluxes from the surface of the world's oceans to the atmosphere are important energy sources for the atmosphere. Momentum flux between the atmosphere and oceans produces a wind stress on the ocean surface that drives most ocean currents. These are parameterized according to bulk aerodynamic schemes in which the flux is assumed to be proportional to the surface wind speed and the potential (moisture or temperature difference between ocean surface and air near the surface). The coefficient of proportionally or drag coefficient is determined by an empirically determined functional fit. Over the ocean surface the functional fit is similar to that shown in Sato et al. (1989b):

$$C_m = \frac{1}{F_m^2}; \quad C_h = \frac{1}{F_m F_h} \qquad (36)$$

$C_m$ and $C_h$ are multiplied by the magnitude of the wind velocity to yield the drag coefficients for momentum and heat/moisture transfer. The functions $F_m$ and $F_h$ are determined as follows. First, set

$$F_m^0 = F_h^0 = 2.1895 \ln\left(\frac{z_r}{z_0}\right) - 1.5630 \qquad (37)$$

In the stable region: $R_i > 0$

$$\frac{F_m}{F_m^0} = \frac{F_h}{F_h^0} = \exp\left\{-1.89 + \left[(1.89)^2 + 5.0519x\right]^{1/2}\right\} \qquad (38)$$

where

$$x = \ln(1.0 + 10.815\ R_i)$$

For the unstable region: $Ri < 0$

$$\frac{F_m}{F_m^0} = \exp\left\{1.2270 - \left[(1.2270)^2 + 1.2642\,x\right]^{1/2}\right\} \qquad (39)$$

where

$$x = \ln(1. - 1.2743Ri)$$

and

$$\frac{F_h}{F_h^0} = \exp\left\{-1.89 + \left[(1.89)^2 + 5.0519x\right]^{1/2}\right\} \qquad (40)$$

where

$$x = \ln(1.0 - 3.4805Ri)$$

In the above formulae, $z_r$ is the reference height, $z_0$ is the roughness length and $Ri$ is the bulk Richardson number. This approach, which differs from the Monin and Obukhov formulation, was adopted to improve computational efficiency.

Sea ice points are treated differently. The temperature of the sea ice is computed by solving the following equation:

$$\rho c_i \Delta z_i \frac{\partial T_s}{\partial t} = R_{\downarrow} - \rho c_p c_h (T_s - T_1 \sigma_1^{-\kappa}) - \rho L c_h (q_s - q_1) - c_c (T_s - T_i) - \sigma T^4 \qquad (41)$$

Where the subscript, *i*, refers to ice and the subscript, *1*, refers to the lowest $\sigma$ level of the model. Fluxes and values of model variables from the previous time step are used to estimate the new values, the drag coefficients are recomputed, and the new sea ice temperature is then computed.

B. Land

The land surface of the Earth is composed of a variety of different plants, soil and geographical formations, all of which exchange mass, momentum and heat with the atmosphere through

several processes in varying degrees. Many studies have shown the differences in various fluxes between the land surface and the atmosphere depend upon whether the fluxes are measured over bare soil or over vegetated areas. Further refinement of the dependence of the fluxes on vegetation type has also been achieved. The fluxes which are most significantly dependent upon the vegetation type are the radiative flux (e.g., Charney et al., 1977), the latent heat flux (e.g., Shukla and Mintz, 1982), and the momentum flux (e.g., Sud and Smith, 1985). It has been shown that seasonal simulation of the atmospheric circulation near the surface depends heavily upon the nature of the surface fluxes, particularly of latent heat (Sato et al., 1989a). Other studies have shown that the latent heat flux has a direct bearing upon the accuracy of the short to medium range forecast of surface temperature and humidity (Shukla et al., 1990). As a result of these studies, the COLA GCM includes an explicit formulation of the land surface vegetation and its exchanges with the atmosphere that is based on the Simple Biosphere model (SiB) of Sellers et al. (1986). The SiB model was simplified by Xue et al. (1991), and is now referred to as the Simplified SiB model (SSIB). The following describes SSIB as it is used in the COLA GCM.

Simplified SiB(SSIB) Model:

In SSIB, the following processes are taken into account:

- selective absorption of photosynthetically active radiation (PAR);
- root and stomatal resistance to water vapor fluxes from the soil to the atmosphere;
- storage, drainage and evaporation of intercepted precipitation and dew from plant surfaces;
- runoff of excess precipitation and drainage of ground water;
- thermal and radiative effects of snow cover on the ground and canopy surfaces; and
- the influence of different plant morphologies on roughness length, and hence transfer of momentum, heat and moisture between land and atmosphere.

As shown by Sato et al.(1989a), using a realistic treatment of atmosphere-biosphere interaction leads to:

- an improved calculation of the Bowen ratio between energy fluxes of latent and sensible heat from the land surface to the atmosphere; and consequently,
- an increase in the Bowen ratio relative to non-biophysical formulations (e.g., the "bucket" model of Manabe, 1969), a decrease in precipitation over land, and a realistic diurnal cycle of surface air temperature and planetary boundary layer depth over land.

The vegetation-soil layer affects the radiative transfer at the surface, the partitioning of surface energy into sensible heat flux and latent heat flux and the transfer of momentum between land and atmosphere. SSiB is intended to realistically simulate the biophysical exchange processes. The biophysical controls on these exchange processes are modeled in a mutually consistent manner by representing the effects of vegetation explicitly. Each COLA GCM land grid point is assigned one of 12 vegetation types (or permanent ice cover), whose physical and morphological properties are specified and are dependent upon the time of year (Dorman and Sellers, 1989).

The development of SSIB was based upon observational data from the Amazon rain forest (Xue et al., 1991). A number of observational data sets from different sites and vegetation types have been used to validate and evaluate this model, including data from: the Anglo-Brazilian Amazonian Climate Observation Study (ABRACOS) - a field experiment over an Amazon

deforestation site (Xue et. al., 1996); the Sahelian Energy Balance experiment (SEBEX) - a field experiment over a semi-arid region (Xue and Allen, 1995); the First ISLSCP field experiment (FIFE) in Kansas (F. Chen et al., 1995); the series of Russian hydrological measurements (Robock et al., 1995, Schlosser, 1995); the Cabauw experiment on a grassland site in Netherlands (T. Chen et al., 1995b); and the Hapex-Mobilhy field experiment - a series of observations in a cultivated (soya) field mixed with coniferous forest (Xue et al., 1996b). Most of the following description of SSiB is taken from Xue et al. (1996a and 1996b).

SSiB has three soil layers and one canopy layer, and eight prognostic variables: soil wetness in the three soil layers; temperatures at the canopy, ground surface and deep soil layers; water stored on the canopy, and water (liquid or frozen) stored on the ground (Fig. 2). The governing equation for canopy temperature $T_c$ is based on the energy conservation equation:

$$C_c \frac{\partial T_c}{\partial t} = R_{nc} - H_c - \lambda E_c \qquad (42)$$

where $C_c$, $R_{nc}$, $H_c$, and $\lambda E_c$ are the heat capacity of the canopy, and the net radiation, sensible heat, and latent heat fluxes at the canopy level, respectively. In the radiative transfer submodel, the optical and geometric properties of the leaves and stems, and the optical properties of the soil affect the surface albedo and the attenuation of photosynthetically active radiation (PAR) down through the canopy. The surface albedo is modeled to have a diurnal variation with a minimum at local noon. Since the variation of the albedo with solar angle is quite regular, a quadratic equation is used to describe the albedo and its diurnal variations. The equation was fitted to the results of two-stream radiative transfer model calculations. For a specific vegetation type, the albedo $\alpha$ is also a function of the solar zenith angle $\theta$ and snow cover $S$:

$$\alpha = a\cos\theta + b(\cos\theta)^2 + cS + dS^2 + e \qquad (43)$$

The coefficients of the quadratic equation ($a,b,c,d$, and $e$) depend on vegetation type.

The force-restore method is used to predict the time variation of the soil temperature $T_{gs}$ within a shallow layer where the diurnal cycle of temperature predominates:

$$C_{gs} \frac{\partial T_{gs}}{\partial t} = R_{ngs} - H_{gs} - \lambda E_{gs} - \frac{2\pi C_{gs}}{\tau}(T_{gs} - T_d) \qquad (44)$$

where $\tau$ is the day length, $C_{gs}$ is the effective heat capacity of soil, $T_d$ is the temperature for deep soil, and $R_{ngs}$, $H_{gs}$, and $\lambda E_{gs}$ are net radiation, sensible heat, and latent heat fluxes at the ground, respectively. The equation for deep soil temperature, $T_d$ , representative of the soil layer dominated by the annual cycle is:

$$C_d \frac{\partial T_d}{\partial t} = \frac{2\pi C_{gs}(T_{gs} - T_d)}{\tau\sqrt{365\pi}} \qquad (45)$$

The depths at which $T_{gs}$ and $T_d$ are computed are unspecified, and actually vary in space and time as a function of soil properties and soil moisture, through variations in heat capacity.

The governing equation for the canopy interception water store $M_c$ is based on water mass conservation:

$$\frac{\partial M_c}{\partial t} = P_c - D_c - E_{wc} \qquad (46)$$

where $P_c$, $D_c$, and $E_{wc}$ are the precipitation rate, water drainage rate, and evaporation rate from the wetted portions of the vegetation canopy, respectively. The canopy has a maximum instantaneous water store of *(1/10 LAI)* mm liquid water equivalent. The governing equation for snow depth $M_S$ is

$$\frac{\partial M_s}{\partial t} = P_s - S_m + W_f \qquad (47)$$

where $P_S$, $S_m$, and $W_f$ are snowfall, snow melt, and the freezing of water, respectively.

The water that accumulates on the ground and canopy surfaces may be in either liquid or solid form (snow). As precipitation nears the ground in the model, it is assumed to instantly equilibrate with the air at the reference temperature, $T_r$. If $T_r$ is below freezing, then the precipitation is assumed to be snow. If the temperature of the vegetation canopy or the ground surface is below freezing, water storage on the ground is assumed to be frozen and accumulates. Snow is assumed to accumulate entirely on the ground. Once snow has accumulated, if $T_r$ rises above freezing, then the snow begins to melt. If the temperature at either one of the two subsurface model levels is above freezing when snow is melting, then the meltwater infiltrates into the ground. If the surface layer soil moisture becomes saturated, then meltwater runs off. Finally, if snow is melting but both subsurface temperatures are below freezing, then meltwater is assumed to run

off. Snow accumulation on the ground thus has a direct effect on the GCM surface hydrologic balance. Snow increases the surface albedo substantially in the model. Snow also significantly alters the partitioning of the surface latent and sensible heat fluxes in favor of the latent heat flux. The effects of sublimation, cloud physics, and blowing snow are neglected in the model. The initial value of snow depth is specified based on observations (see section VIIA).

In the three soil layers, water movement is described by a finite-difference approximation to the diffusion equations:

$$\frac{\partial \theta_1}{\partial t} = \frac{1}{D_1}[I - Q_{12} - (E_{gs} + b_1 E_{dc})] \qquad (48)$$

$$\frac{\partial \theta_2}{\partial t} = \frac{1}{D_2}[Q_{12} - Q_{23} - b_2 E_{dc}] \qquad (49)$$

$$\frac{\partial \theta_3}{\partial t} = \frac{1}{D_3}[Q_{23} - Q_3 - b_3 E_{dc}] \qquad (50)$$

where $\theta_1$, $\theta_2$, $\theta_3$, $D_1$, $D_2$, and $D_3$ are the volumetric soil water content and soil thickness of the top, middle, and lower soil layers, respectively. The term $I$ is the infiltration where $I = D_c - R_u$ ($R_u$ is the instantaneous surface runoff). The variable $E_{dc}$ is the transpiration rate, and $E_{gs}$ is the evaporation from bare soil. The coefficients $b_i$ (i=1,2,3) are fraction factors which depend on the root distribution. $Q_{i,j}$ is the transfer of water between the *ith* and *jth* layers and is defined to be positive upward as:

$$Q_{i,j} = \left[ k \frac{\partial \psi}{\partial z} + 1 \right] \qquad (51)$$

where $k$ is the hydraulic conductivity, $\psi$ is the soil water potential, and $z$ is the thickness between two soil layers. The soil water potential in SSiB is taken from the empirical relationship of Clapp and Homberger (1978):

$$\psi = \psi_s \left( \frac{\theta}{\theta_s} \right)^B \qquad (52)$$

where $\psi_s$ is the volumetric soil water content at saturation and the $B$ parameter is an empirical constant dependent on the soil type. The drainage of water out of the bottom layer is:

$$Q_3 = k_3 \sin\kappa + Q_b \qquad (53)$$

The first term of the right hand side is contributed by gravity only, with no diffusive transport occurring, as modeled by Sellers et al. (1986). The variable $\kappa$ is the mean slope angle and set to larger than 3° and $k_3$ is the hydraulic conductivity of the third layer, and $Q_b$ is the base flow runoff and is proportional to the soil wetness in the lowest soil layer, $Q_b = K_c * (\theta_3/\theta_s)$. $\theta_3$ is the volumetric soil water content in the third soil layer. This term was suggested by Liston et al. (1994) to account for the GCM sub-grid scale variation of soil moisture. The empirical constant $K_c$ is derived from large river basins. The hydraulic conductivity at layer $i$, $k_i$, is

$$k_i = k_s\left(\theta_i / \theta_s\right)^{(2B+3)} \qquad (54)$$

where $k_s$ is the hydraulic conductivity at saturation. The logarithm of $k$ decreases linearly as $B$ increases. Hydraulic conductivity changes more dramatically with $B$ in the dry soil than in the wet soil; and has a larger variation with soil moisture when $B$ is large.

The parameterization of the stomatal resistance, $r_c$, in SSiB was based on the work of Jarvis (1976). Three stress terms are included in this scheme which describe the dependence of stomatal resistance on atmospheric temperature, soil water potential, and vapor pressure deficit. Unlike the traditional approach in which the leaf water potential is used to calculated the stomatal resistance (Federer, 1979), soil moisture is used to control stomatal resistance in SSiB. Using leaf water potential makes the computation very complex and a large number of parameters are required. Evidence (Blackman and Davies; 1985, Wetzel and Chang, 1987) indicates that the stomatal response to water supply is not controlled by the plant's internal water potential. Instead, it appears that roots "sense" the soil moisture supply and directly transmit chemical messages (cytokinin) to the guard cells to keep stomata open. Thus, stomatal closure occurs in direct response to soil moisture and is not delayed while a plant's internal water supply is squandered. The empirical formula for the adjustment factor $f(\psi)$ for soil water potential is:

$$f(\psi) = 1 - \exp\{-c_2[c_1 - \ln(-\psi)]\} \qquad (55)$$

where $c_2$ depends on the vegetation type and $c_1$ is a constant which is obtained using the wilting point. The stomata completely close at the wilting point in the model. The variable $c_2$ is a slope factor; a large value of $c_2$ means that $f(\psi)$ changes from 0 to 1 very fast when soil water content varies from the wilting point to the point stomata start to close. Note that in Table 1 of Xue et al. (1991) the values of $c_1$ and $c_2$ should be interchanged.

The equation for transpiration from the canopy is:

$$E_t = \frac{(q(T_c) - q_a)}{r_c + r_b}(1 - w_c) \qquad (56)$$

where $q(T_c)$ and $q_a$ are the saturated specific humidity at the canopy temperature and specific humidity of the canopy air space, respectively. The term $r_b$ is the bulk boundary layer resistance, $r_c$ is the stomatal resistance, and $w_c$ is the wetness fraction of the canopy. Bare soil evaporation in the model is given by:

$$E_s = \frac{[f_h q(T_{gs}) - q_a]}{r_{surf} + r_d}(1 - V_g) \qquad (57)$$

where $q(T_{gs})$ is the saturated specific humidity at the surface temperature $T_{gs}$, and $V_g$ is the vegetation cover. The resistance to the transfer of water vapor from the upper soil layer to the canopy air space includes aerodynamic resistance $r_d$ and soil surface resistance $r_{surf}$ (Fig. 1). The results of Camillo and Gurney (1986) were used to fit a simple relationship between soil surface resistance and soil moisture in the first layer:

$$r_{surf} = 101840\left[1 - \left(\frac{\theta_1}{\theta_s}\right)^{0.0027}\right] \qquad (58)$$

The relative humidity of the air at the soil surface is:

$$f_h = \begin{bmatrix} \exp\left(\frac{\theta_1 g}{T_{gs}} R_v\right) & q_a < q(T_{gs}) \\ 1 & otherwise \end{bmatrix} \qquad (59)$$

As usual, $g$ is the acceleration due to gravity and $R_V$ is the gas constant for water vapor. Similarity theory was used to calculate the aerodynamic resistance from the canopy to the reference height. Based upon the equations of Paulson (1970) and Businger et al. (1971), a linear relationship between the Richardson number and the aerodynamic resistance was developed. The equation for momentum flux transfer is:

$$U_* = U_r(C_u^{-1} + C_{um}^{-1}) \qquad (60)$$

where $U*$ is the friction velocity, $U_r$ is the wind velocity at the reference height, $C_{un}$ is the neutral momentum transfer coefficient, and $C_u$ is the non-neutral coefficient. Louis (1979) developed a parameterization scheme in which the total aerodynamic resistance including both neutral and non-neutral parts is a function of Richardson number and surface roughness. The accuracy of this parameterization strongly depends on the surface roughness length. In a biosphere model, the range of values of surface roughness length can by very large. Parameterizing the total resistance may cause large errors. In SSIB, we only parameterize the non-neutral part; $C_{un}$, which is dependent on vegetation and soil properties, is given by:

$$C_{um}^{-1} = \frac{1}{k_0} ln\left(\frac{z_m - d}{z_0}\right) \qquad (61)$$

where $k_0$ is von K×rm×n's constant, $z_m$ is the reference height, $d$ is the displacement height, and $z_0$ is the roughness height. For the non-neutral part,

$$C_u^{-1} = \begin{bmatrix} 0.315\,Ri, & -10 \le Ri < 0 \\ 66.85\,Ri, & 0 \le Ri \le 0.16 \end{bmatrix} \qquad (62)$$

and

$$Ri = \frac{g\Delta z \Delta\theta}{\theta(\Delta u)^2} \qquad (63)$$

where $u$ is the wind speed and $\theta$ is the potential temperature. Xue et al. (1991) fitted an exponential equation to relate the bulk Richardson number to surface resistance that reproduces the results of similarity theory. Eddy flux in each grid point in a GCM is assumed to be the average of the influence of a large number of sub-grid-scale eddies. Sud and Smith (1985) found that the relationship between aerodynamic resistance and ensemble mean Richardson number had a tendency to change from exponential to linear. The linear parameterization described here has produced very good flux simulations in many cases (e.g., Shao et al. 1994). The equations for heat flux transfer are:

$$E = \frac{U_*}{(C_{TN}^{-1} + C_{TT}^{-1})}(q_m - q_a) \equiv \frac{(q_m - q_a)}{r_a} \qquad (64)$$

for latent heat flux, $E$, and

$$F = \frac{U_*}{(C_{TN}^{-1} + C_{TT}^{-1})}(T_m - T_a) \equiv \frac{(T_m - T_a)}{r_a} \qquad (65)$$

for sensible heat flux, $F$. Variables $T_m$, $q_m$, $T_a$, and $q_a$ are the temperatures and specific humidity at the reference height and in the canopy air space, respectively. Parameter $C_{TN}$ is the neutral heat transfer coefficient and $r_a$ is the aerodynamic resistance. Coefficient $C_{TN}$ is given by

$$C_{TN}^{-1} = \frac{1}{k_0}\left( ln\frac{z_m - d}{z_r - d} + g_3 ln\frac{z_r - d}{z_2 - d} \right) \qquad (66)$$

where $z_2$ is the height of the canopy and $g_3$ is the ratio of actual $r_a$ to $r_a$ calculated using a log-linear wind profile assumption. It is held constant at 0.75. The depth of the transition layer above the canopy is $z_r$. Above this transition layer, the log-linear assumption is valid. Following Sellers et al. (1989), we use:

$$z_r = z_2 + 11.785\, z_0 \qquad (67)$$

For the non-neutral heat transfer coefficient, we have:

$$C_{IT}^{-1} = f\,[Ri\,(z_m)] + (g_3 - 1)\, f\,[Ri\,(z_r)] - g_3\, f\,[Ri\,(z_2)] \qquad (68)$$

for $0 > Ri > -10$, where

$$f(Ri) = 0.94\, Ri.$$

For $0.16 > Ri > 0$, we have:

$$C_{IT}^{-1} = 66.85\, Ri\,(z_m)$$

$$X\left[1 + \frac{z_r - d}{z_m - d}(g_3 - 1) - g_3 \frac{z_2 - d}{z_m - d}\right] \qquad (69)$$

## IV. Planetary Boundary Layer

A. Vertical diffusion - Mellor-Yamada closure scheme

The effects of mixing of heat, momentum and moisture by small scale turbulence is represented by vertical diffusion in the COLA GCM. The mixing coefficients are calculated according to the "level 2.0" closure scheme of Mellor and Yamada (1982). This method assumes a local balance between production and dissipation of turbulent kinetic energy. There are no explicit prognostic variables to describe the planetary boundary layer (PBL); instead, the entire atmosphere is represented in discrete layers which may or may not be part of the PBL. The prognostic equations for atmospheric temperatures and moisture are then coupled to the SSIB equations for the ground surface and canopy, and the system of coupled equations is solved simultaneously with vertical diffusion of heat, moisture, and momentum as given by the Mellor and Yamada (1982) scheme.

In the turbulence closure method, each prognostic variable is expressed as a sum of a large scale (resolved) part and a turbulent (sub-grid) scale part. The vertical fluxes that are expressed as quadratic terms in the turbulent quantities are assumed to be represented by vertical diffusion down the gradient of the large scale quantities, e.g.

$$-\overline{(uw)} = K_M \frac{\partial U}{\partial z} \qquad (70)$$

where $u$ and $w$ are the turbulent zonal and vertical velocity components, $U$ is the large scale zonal velocity components and $K_M$ is a momentum diffusion coefficient. The overbar denotes averaging on the large (grid) scale, and $z$ represents the vertical direction coordinate. The turbulence closure method involves two assumptions. (1) The diffusion coefficients are expressed as:

$$K_M = lq\, S_M \qquad (71)$$

$$K_H = lq\, S_H \qquad (72)$$

where $K_M$ and $K_H$ are the diffusion coefficients for momentum and heat, respectively, $l$ is the master turbulence length scale, $q^2$ is the turbulent kinetic energy (so $q$ is the magnitude of the turbulent wind velocity), and $S_M$ and $S_H$ are momentum flux and heat flux stability parameters, respectively. The ratio of $S_H$ to $S_M$ is equal to the ratio of the turbulent flux Richardson number to the bulk (large scale) Richardson number. $K_M$ and $K_H$ are constrained, viz.

$$1 \leq K_M \leq 300$$

$$0.1 \leq K_H \leq 300$$

and (2) The turbulent kinetic energy (TKE) equation is closed by assuming that production and dissipation of TKE is balanced instantaneously at each point. This assumption leads to a system of equations for $l$, $q$, $S_M$, and $S_H$ that may be solved simultaneously to give vertical diffusion coefficients used to couple the discrete layers of the GCM and the surface layers in SSiB.

B. Gravity wave drag

The parameterization of gravity wave drag (GWD) is based on simplified theoretical concepts and observational evidence. The parameterization consists of determines the drag due to gravity waves at the surface and its vertical variation. We have adopted the scheme of Alpert et al. (1988) as implemented by Kirtman et al. (1992). The parameterization of the drag at the surface is based on the formulation described by Pierrehumbert (1987) and Helfand et al. (1987).

The momentum flux due to the gravity waves averaged over a grid box is written as

$$\vec{\tau}_{gw} = < \rho \vec{V}' w' > \qquad (73)$$

where $\rho$ is the density of air and $V'$ and $w'$ are the fluctuations in the horizontal wind vector and vertical velocity due to gravity waves, respectively. The angle brackets indicate an average over the model grid box. The GWD due to this momentum flux is then an additional body force on the atmosphere. That is,

$$\frac{\partial \vec{V}}{\partial t} + ... + = \frac{1}{\rho}\frac{\partial \vec{\tau}_{gw}}{\partial z} = -\frac{g}{p_s}\frac{\partial \vec{\tau}_{gw}}{\partial \sigma} \qquad (74)$$

Pierrehumbert (1987) argued that convective instability and wave breaking at the Earth's surface are so prevalent that nonlinear effects become very common and cannot be neglected. Based on scaling arguments and the results from numerical experiments, Pierrehumbert (1987) obtained a formula for the surface wind stress due to gravity waves. He concluded that

$$|\vec{\tau}_{gw}| = \frac{\rho U^3}{Nl^*}\left[\frac{F_r^2}{1+F_r^2}\right] \qquad (75)$$

where $F_r = Nh/U$ is the Froude number, $N$ is the Brunt-Vaisala frequency, $U$ is the surface wind speed, $h$ is the amplitude of the orographic perturbation, $l^*$ is the wave length of the monochromatic wave in the direction of the surface wind and $\tau_{gw}$ is in the direction of the surface wind.

The equation for the surface wind stress is valid for a wide range of values of the Froude number, in particular for $F_r < 0.8$ for which the linear theory is valid, and for $F_r > 0.8$ where nonlinear

effects become important. On the other hand, the momentum flux due to the gravity waves above the wave breaking level increases linearly with Froude number even for $F_r > 0.8$. Assuming that the momentum flux due to the gravity waves does not change with height below the breaking level, the difference between the surface drag, which equals $\tau_{gw}$ below the breaking level, and the momentum flux due to the gravity waves above the breaking level is proportional to the wave drag in the intervening layer. Consequently, in the nonlinear range, the momentum deposition within the breaking layer is much larger than in the linear range.

To account for the nonlinear amplification of the surface drag, a base layer is defined to compute $\tau_{gw}$ at the surface. The base layer is approximately the lowest one third of the model atmosphere. The equation for the surface stress is computed by using mass weighted variables over the depth of the base layer. In the COLA GCM, $l^* = 125$ km and $h$ equals the subgrid scale standard deviation of the orography. The standard deviation is computed from the Navy 10' by 10' orography data by taking departures from the mean orography of the model grid. As in other studies, the computed $h$ is constrained to 400 m for numerical stability. This constraint is based on the assumption that the Coriolis acceleration is at least one order of magnitude larger than the acceleration due to gravity wave drag (see Helfand et al., 1987).

As shown by Eliassen and Palm (1961), $\tau_{gw}$ is independent of height in the absence of turbulent dissipation or transience. In such a case, the parameterization deposits the momentum in the top layer of the model and hence there is no body force on the atmosphere in the remaining lower layers because $\partial \tau_{gw}/\partial \sigma = 0$.

On the other hand, the value of $\tau_{gw}$ changes in the vertical when the local value of the wave modified Richardson number, $Ri_m = Ri\ (1-F_r)$ is less than or equal to 0.25. Wave breaking occurs at levels where amplification of the wave causes the local Froude number to exceed a critical Froude number, $F_{rc} = (1 - 1/4Ri)$. If such a condition holds, the wave saturation hypothesis of Lindzen (1981) is invoked and wave induced turbulence reduces the magnitude of $\tau_{gw}$. Finally, $\tau_{gw}$ vanishes when a critical level, convective instability, or shear instability is encountered. Critical levels occur where $V \cdot V_{surface} < 0$. Shear instability, where $Ri < \frac{1}{4}$, creates turbulence and, according to Eliassen and Palm (1961), the momentum flux vanishes at that level. In order to allow the gravity wave effects to propagate above the base layer, it is assumed that $\tau_{gw}$ can change in the base layer only due to wave saturation and not by the occurrence of critical levels or instabilities.

## V. Moist Processes

In the semi-implicit treatment of the moisture equation (5), the contributions to the moisture tendency are further split into two groups. First, the moisture tendency due to advection, surface fluxes and diffusion is computed, and a preliminary calculation of the moisture field at the next time step is made based on this tendency. Second, the moisture sources and sinks due to changes of phase are computed and a final determination of moisture at the next time is made. Changes of phase of water rank highly among the important processes affecting the dynamics and thermodynamics of the atmosphere. In the COLA GCM, we include the processes of large scale condensation, deep convection and shallow convection.

### A. Large scale condensation

The change of phase of water is one of the very important processes that affect both the dynamics and thermodynamics of the atmosphere. As an air parcel containing water vapor is cooled, its capacity to retain water is reduced until the parcel is saturated (100% relative humidity). If the parcel is cooled any further, water vapor will change phase to liquid, releasing its latent heat of evaporation and forming a cloud. While this is a complex process involving the availability of cloud condensation nuclei, it is treated quite simply in the COLA GCM. Whenever the predicted moisture content in a given volume exceeds the saturation value, the excess water vapor is assumed to condense to liquid and precipitate out. The calculation is carried out from the topmost layer of the model to the bottom, including the possibility that liquid water may evaporate at intermediate model levels as described in MRF88 (chapter 5).

### B. Deep convection

Not all condensation takes place simply by supersaturation of gridbox size volumes; most of the mass of water that is condensed in the atmosphere does so in relatively small scale convective clouds. A number of convection parameterizations have been tested with the COLA GCM including a modified Kuo scheme (Kuo, 1965; Anthes 1977; MRF88), the Betts-Miller scheme (Betts and Miller, 1986; 1993), and the relaxed Arakawa-Schubert scheme (RAS; Moorthi and Suarez, 1992). Both the Kuo-based and RAS schemes are available with the COLA GCM. The RAS scheme is currently considered the most suitable for climate simulations with the COLA GCM (DeWitt, 1996).

#### *1. Kuo Scheme*

Heating and moistening due to deep convective clouds can be represented in the COLA GCM using the Kuo (1965) scheme, as modified by Anthes (1977). Deep convection in the Kuo scheme is active in the presence of a conditionally unstable column and a positive moisture source due to the sum of convergence of moisture into the column and evaporation into the column. The sum of the moisture converging into the column and the evaporation into the column is known as the moisture accession.

In those columns for which deep convection is diagnosed, the moisture accession is partitioned into a heat producing (rain producing) portion and a moistening portion based on the column integrated relative humidity. The vertical distribution of the heating and moistening of the

environment is based on the vertical distribution of temperature and specific humidity differences between the cloud and the environment.

The cloud temperature and specific humidity are determined by lifting an air parcel from the lowest model layer dry adiabatically up to the lifting condensation level (cloud base) and then moist adiabatically up to the level where the cloud temperature is equal to the temperature of the environment (cloud top). If the lifting condensation level for the near surface air is not within 0.35 times the surface pressure, then no deep convection is allowed to occur. The moisture accession is determined by computing the change in specific humidity over the leapfrog time step for all levels. The presence of deep convection is further restricted by the following criteria:

- Deep convection only occurs for columns in which the cloud thickness is equal to 30 percent of the surface pressure. For a surface pressure of 1000 mb this would restrict deep convection to those columns which had convective clouds at least 300 mb thick.

- The moisture accession in the layers below $\sigma = 0.46$ must exceed 2 mm $day^{-1}$ on any particular time step in order for deep convection to occur.

*2. Relaxed Arakawa-Schubert*

An alternative to the Kuo scheme in the COLA GCM is the relaxed Arakawa-Schubert (RAS) scheme of Moorthi and Suarez (1992). This scheme differs from the common implementation of the Arakawa and Schubert (1974) scheme following Lord et al. (1982) in two ways. First, the normalized mass flux that is an exponential function of height in the original formulation is replaced by a linear function of height. Second, the parameterization relaxes the large scale atmosphere toward quasi-equilibrium instead of requiring quasi-equilibrium each time the cumulus convection subroutine is called.

The implementation of RAS in the COLA GCM assumes the sub-cloud layer is composed of a mass weighted average of the two lowest model levels. Each time the cumulus convection is called, all levels above the sub-cloud layer are checked for the possibility of convection. Clouds with the same specified cloud base but different detrainment levels (cloud tops) are known as different cloud types. In the RAS scheme, cumulus convection occurs for those cloud types for which the cloud work function exceeds an empirically determined critical value. The cloud work function is an integrated measure of the difference between the moist static energy in the cloud and that in the environment. For those cloud types for which the cloud work function exceeds the critical cloud work function, the cloud base mass flux needed to restore the cloud work function to its critical value is diagnosed. This mass flux is used to solve equations for the grid scale effect of convection on the temperature and specific humidity. In the implementation of RAS in the COLA model, the convective rainfall re-evaporates back into the environment following a modified version of Sud and Molod (1988).

C. Shallow convection

In regions where the atmospheric column is conditionally unstable near the surface, vertical overturning on sub-grid scales may be induced. The resultant shallow cumulus clouds do not necessarily produce precipitation, but act to transport heat and moisture upward. In regions where

the atmospheric column is conditionally unstable near the surface but deep convection does not occur, shallow cumulus clouds may act to mix the temperature and moisture between cloud base and cloud top. This shallow convection is parameterized following Tiedtke (1983). In the Tiedtke (1983) scheme, the effects of shallow convection on temperature and specific humidity are modeled using an eddy diffusivity approach with fixed coefficients. The occurrence of shallow convection is not dependent on the presence of moisture accession into the column. The following restrictions on the shallow convection apply when the deep convection scheme is Kuo:

- Cloud base is determined using the lifting condensation level from the deep convection subroutine, which is called first.
- Shallow convection is not allowed in columns in which deep convection has occurred in the current time step.
- The shallow convective cloud top is restricted to $\sigma$ levels between 0.7 and 1.0. Shallow convective cloud tops that exceed this value are set to the highest layer that meets this criterion.
- The shallow convection cloud base must occur between $\sigma$ levels 0.7 and 1.0.

## VI. Initial Conditions

### A. Spectral analyses

The source of initial conditions for all integration carried out with the COLA GCM is a global gridded analysis of the atmospheric state. Such an analysis is usually taken from the operational products provided by the NCEP (Kanamitsu, 1989; Kanamitsu et al., 1990) or the European Centre for Medium Range Weather Forecasts (ECMWF; Bengtsson et al., 1982; Anderson et al., 1991; Trenberth, 1992). Several centers (NCEP, GSFC, ECMWF, GFDL, and COLA) have reassimilated observational data taken from previous periods (Kalnay et al. 1996; Paolino et al., 1994; Gibson et al., 1997; Schubert et al., 1993), and some of these reanalyses have been used for some COLA GCM integrations. In any case, a basic requirement for integrating the COLA GCM is to start from a global, spectral analysis based on a global gridded analysis. It is beyond the scope of this document to include a description of the assimilation systems used to produce these analyses.

### B. Nonlinear normal mode initialization

Gridded global analyses, by the nature of the assumptions which are employed to make such analyses, may include finite amplitude gravity waves which are almost certainly unresolved and which are certainly beyond accurate reach of the current observing system. For example, spurious gravity wave noise is introduced into the analyses because the several polar orbiting satellite passes, which are made in a given six hour data assimilation period, are assumed to be valid at the time of the analysis, so that a given observation may be aliased by as much as three hours. Because the COLA GCM dynamics can support such gravity waves, it is important to reduce or eliminate the spurious signals introduced by the assimilation process. The method employed to eliminate the noise is called nonlinear normal mode initialization (NNMI - Machenauer, 1977; Baer and Tribbia, 1977). The application of NNMI in the COLA GCM closely follows that described in MRF88. In the following section, the manner in which the heating tendencies are included is described.

### C. Inclusion of heating

In developing the separable primitive equations for NNMI purposes, both the terms which are nonlinear in deviations from the resting basic state and those which force the thermodynamic equation (heating) are maintained on the right hand side. Implicitly, then, while iterating in the Machenauer (1977) scheme, both the nonlinearity and heating could be included in the forcing function. This is carried out in practice by integrating the COLA GCM several time steps (using uninitialized analyses as initial conditions) to compute a mean heating rate. This heating rate is included on the right hand side in each iteration of the NNMI scheme, as in MRF88. The effect of the inclusion is to allow a more realistic divergent circulation in the tropics (largely driven by heating) to be represented in the initial conditions.

## VII. Boundary Conditions

### A. Lower Boundary Conditions

In order to represent atmospheric processes on climate time scales of one month and longer, the conditions at the Earth's surface that most significantly affect the atmosphere must be allowed to vary with time. These fields include surface temperature over land and ocean, including both open water and sea ice; soil moisture over land; surface albedo; and snow depth. Of these fields, the land surface temperature, sea ice temperature, and snow depth vary so quickly with time that they are treated as prognostic variables in the model and are coupled with the atmospheric equations. The remaining fields could also become prognostic fields as well but vary slowly enough that they can be specified as boundary conditions for the model, being allowed to vary independently in time. By doing so, the atmospheric response to these fields can be determined without taking into account the storage residual in each of these fields. As knowledge of these fields and the corresponding atmospheric response increases, they may be also become prognostic variables.

Sea Surface Temperature:

The sea surface temperature (SST) is determined on a daily basis in the model by linear interpolation between means on monthly, weekly or other intervals. These fields are read in from data sets, whose preparation is discussed below. The observed value of SST is modified at each gridpoint of the model by a time invariant correction to account for the non-zero elevation introduced at some ocean points by the spectral truncation of the model orography. The correction is computed as the product of the orography and a constant lapse rate of $6.5°\ K\ km^{-1}$. The monthly mean value from such a data set gives the model field value assumed to be valid instantaneously in the middle of the month. A field value for a day in the first half of the month is obtained by linear interpolation from the monthly means for the previous month and the current month. Similarly, a model field value for a day in the last half of the month is obtained from the monthly means for the current and the subsequent month. In this way a field which is smoothly varying in time can be constructed. Note that this can introduce a smoothing which is not observed and may inaccurately represent the monthly mean fields (Killworth, 1996).

Sea Ice:

For SST, a distinction is needed between open water and sea ice points, and possible transitions from open water to sea ice (and vice-versa) must be taken into account. In the model, this distinction is made when the sea surface is above or below the freezing temperature of sea water (-2°C). With sea ice points for a given month in the monthly sea surface temperature data set assigned to -3°C so that transition between open sea water and sea ice points can be arrived at by the linear interpolation method, each point is checked for its interpolated temperature value. If below -2°C, it is assumed to be a sea ice point, and the temperature at that point is treated as a prognostic variable whose initial value is -3°C. Once it is above -2°C, the time interpolated sea surface temperature is used at that point. The transition from open water to sea ice is done when the time interpolated temperature at a point falls below -2°C. The point remains a sea ice point until the time interpolated sea surface temperature rises above -2°C. The point is then set to the time interpolated sea surface temperature and the previously predicted sea ice temperature valid at the time is ignored.

Albedo

The surface albedo is obtained differently over land and ocean points. Over ocean points, albedo is specified as a function of solar zenith angle:

$$\alpha = 0.12347 + \gamma(0.34667 + \gamma(-1.7485 + \gamma(2.04630 - 0.74839\gamma))) \qquad (76)$$

where $\gamma = \sin(\theta)$ and $\theta$ is the solar zenith angle.

The land surface biosphere model, SSiB, predicts albedo (see section IIIB).

Snow Depth:

The snow depth is applied as an initial condition, and carried as a prognostic variable in the model (see section IIIB). The initial snow depth can be based on the time interpolated surface albedo on the initial date of the model run. The surface albedo normally used to initiate a model integration is a climatological value based on Posey and Clapp (1954). The data are specified on the model Gaussian grid. The initial snow depth is specified as follows:

| | |
|---|---|
| For ice points (both land and sea) | 3000 kg $m^{-2}$ |
| For points where 69%< albedo <75% | 20 kg $m^{-2}$ |
| For points where 49%< albedo <69% | 10 kg $m^{-2}$ |
| For points where 40%< albedo <49% | 5 kg $m^{-2}$ |

The high value over ice points is so that a full account of ice melting or accumulation can be done during a long integration. The initial snow depth is set using an offline program. For boreal summer runs, the ice points alone can be set. It is also possible to use data sets of observed snow depth for particular periods to initialize the model.

Soil Moisture:

Soil moisture is specified initially since the land surface model predicts the soil wetness in each of three layers. The data sets that are used were obtained from the water budget analyses of Willmott et al. (1985), either for climatological monthly means, or for means for a specific calendar month (e.g., April, 1987). The data are available on a 1° by 1° grid, and are interpolated to the model Gaussian grid. The soil moisture data are converted to soil wetness, and distributed over the three soil moisture storage layers maintained within the model as explained in Sato et al. (1989b). A scheme for estimating the initial values of the three soil moisture reservoirs from other soil moisture analyses (e.g., from the European Centre for Medium Range Weather Forecasts) has also been developed (Fennessy and Shukla, 1996).

Sea Surface Temperature Data Sets:

*General Preparation.* All SST data sets used by the COLA AGCM require interpolation to the model Gaussian grid. Currently, areal interpolation is used separately on the SST and sea ice. When a location has an area average sea ice of 50% or more, that location is assigned as a sea ice point with a value of 270.2 K (-3°C). Non sea ice locations have a value of the interpolated SST or 271.4 K, whichever is larger. Due to Gibbs aliasing, SST at locations near land frequently will not be interpreted as originating at sea level. Instead, the SST will be seen as if it were on a surface corresponding to the surface spectral topography transformed to the model Gaussian grid space. This can "raise" the SST to elevations of 3 km or more. To avoid spurious heating, the

SST (sea ice points excluded) is adjusted by the model back-transformed surface topography using the standard atmospheric lapse rate of -6.5 K $km^{-1}$.

*Monthly data sets.* Two types of monthly data sets can be processed by the model: 12 month cyclic sequential data or continuous direct access data. The 12 month cyclic data set consists of 13 records the first of which is no longer used, but remains for backward compatibility. The last 12 records are January through December values of SST assumed to be valid at the center of the month. Data can be climatological or observed. If observed, the data need not align with a calendar year but can start with any month and continue into the following year up to the month corresponding to the calendar month preceding the starting month. Data from each calendar month used, regardless of year, must be in the same data set position as used for a calendar year, i.e., all January data are the second data set record, all February data are the third data set record, until the December data as the thirteenth data set record. Multi-year simulations can be done with this type of data set provided data sets are changed every 10 months to allow for time interpolation. Continuous direct access data sets can contain any number of records of two or more. This avoids the need for changing data sets, but requires the user to indicate the data set start time in the model NAMELIST. This type of data set is not well suited for climatological data.

*COADS/ICE SST climatology.* This climatology is available on a global basis on a 2° by 2° grid, and represents monthly means, averaged over the period (1950-1979). The data set combines the COADS in situ data with the climatological, satellite derived monthly mean ice limits (Reynolds and Roberts, 1987).

*COLA (1982-1994) SST.* This data set contains monthly means of SST and sea ice extent on a global basis for each month starting from January 1982. (As above, the resolution is 2° by 2°). Monthly means were obtained from a blend of satellite and in situ data, and took into account the actual ice edge for the given month (Reynolds, 1988). SST data outside of 60°N to 50°S is set equal to the COADS/ICE SST climatology.

*COLA (1979-1981) SST.* The above month-by-month SST and sea ice data set has been extended backwards in time to January 1979 by M. Fennessy at COLA. This was accomplished by combining the monthly in situ data from Reynolds (1982) for the tropics and extratropics with the COADS global climatology in polar regions. The SST has been made consistent with the observed sea ice limits for each individual month.

*CPC monthly optimum interpolation SST (Nov. 1981 to present).* Starting from the screened weekly optimum interpolation SST (see below) the SST are interpolated each day and the average of these interpolated days during the month is taken. This matches with the procedure used by the Climate Prediction Center (CPC) to produce their monthly OISST data sets, but here sea ice is treated separately. If 50% or more of the daily interpolated values are at the sea ice temperature (-1.8°C) at a given point, that point is treated as a sea ice point and given the sea ice temperature as seen by the model (-3°C). Otherwise, the average daily interpolated value is used.

*Weekly data sets*: At present, only one weekly data set is available for use with the COLA AGCM.

*CPC weekly optimum interpolation SST (Nov. 1981 to present).* Using 1°x1° optimum interpolation SST (OISST) provided by the CPC (Reynolds and Smith, 1995), several steps are taken to prepare the data for the COLA AGCM. First, the

data are screened to establish the minimum SST for each week. This value is normally -1.8°C, but may differ due to truncation errors that occurred during data transfer. All locations with the minimum SST value for that week are assumed to be sea ice points and are assigned the value -1.8°C. This permits the areal interpolation and surface height adjustment program to treat the data consistently. Finally, as recommended by the CPC online documentation, the areally interpolated data are time filtered (ignoring any sea ice points) using a 1-2-1 time filter. Due to satellite source differences, the data fall into two periods: Sunday-centered data from November 1981 through December 1989 and Wednesday-centered data from January 1990 to present. Data in these two periods are time filtered separately. Data that span 1 January 1990 are filtered with the average of the two closest weeks. This requires stopping model integrations at or around 1 January 1990 to change data sets. Otherwise the data set produced is a continuous direct access data set requiring the user to specify the initial starting time in the model NAMELIST. SST is then linearly interpolated at least daily between the adjacent weeks.

B. Upper Boundary Conditions

The upper boundary condition is the kinematic constraint that vertical velocity through the top of the model atmosphere be zero everywhere (to satisfy mass conservation). This constraint is built into the solution through the vertical differencing in $\sigma$ coordinates.

C. Interior (fixed species)

The concentration of ozone is specified by interpolation from a table which gives the ozone mixing ratio for each of the model $\sigma$ levels, for each five degree latitude interval and for each of the four seasons (MRF88). Carbon dioxide, which is a radiatively active gas, is assumed to be well mixed throughout the entire atmosphere with a constant (default) value of 345 ppm (or as specified by the user).

**Acknowledgements**

We are grateful to the National Centers for Environmental Prediction (NCEP) for providing the original computer code for the MRF model in 1985 and for providing initial conditions and boundary conditions data sets that have been used in over a decade of research with the model at COLA. Support for the preparation of this document was provided by the National Science Foundation (ATM-9321354), the National Oceanic and Atmospheric Administration (NA76GP0258), and the National Aeronautics and Space Administration (NAGW-5213).

**References**


Alpert, J. C., M. Kanamitsu, P. M. Caplan, J. G. Sela, G. H. White, and E. Kalnay, 1988: Mountain induced gravity wave drag parameterization in the NMC medium range forecast model. *Proc. Eighth Conf. On Numerical Wea. Prediction,* Baltimore, MD, 726-733.

Anderson, E., A. Hollingworth, G. Kelly, P Lonnberg, J. Pailleux and Z. Zhang, 1991: Global observing system experiments on operational statistical retrievals of satellite sounding data. *Mon. Wea. Rev.*, **119**, 1851-1864.

Anthes, R. A. 1977: A cumulus parameterization scheme utilizing a one-dimensional cloud model. *Mon. Wea. Rev.*, **105**, 270-286.

Arakawa, A., and W. H. Schubert, 1974: Interaction of cumulus cloud ensemble with the large-scale environment. Part I. *J. Atmos. Sci.*, **31**, 671-701.

Arakawa, A., 1972: Design of the UCLA general circulation model. Numerical Simulation of Weather and Climate, Dept. of Meteorology, University of California, Los Angeles, Tech. Rep.7, 116 pp.

Baer, F. and J. J. Tribbia, 1977: On a complete filtering of gravity modes through nonlinear initialization. *Mon. Wea. Rev.*, **105**, 1536-1539.

Barkstrom, B., 1984: The Earth Radiation Budget Experiment (ERBE). Bull. Amer. Meteor. Soc., 65, 1170-1185.

Barkstrom, B., E. Harrison, G. Smith, R. Green, J. Kibler, R. Cess, and the ERBE Science Team, 1989: Earth Radiation Budget Experiment (ERBE) archival and April 1985 results. *Bull. Amer. Meteor. Soc.*, **70**, 1254-1262.

Bengtsson, L., M. Kanamitsu, P. Kallberg and S. Uppala, 1982: FGGE 4-dimensional data assimilation at ECMWF. *Bull. Amer. Meteor. Soc.*, **63**, 29-43.

Betts, A. K., and M. J. Miller, 1993: The Betts-Miller scheme. American Meteorological Society, Meteorological Monograph on Convective Parameterization.

Blackman, P. G. and W. J. Davies, 1985: Root to shoot communication in maize plants of the effects of soil drying. *J. Exp. Bot.*, **36**, 39-48.

Bourke, W., 1972: An efficient, one level primitive equation spectral model. *Mon. Wea. Rev.*, **100**, 683-689.

Businger, J.A., J.C. Wyngaard, Y.I. Zumi, and E.G. Bradley, 1971: Flux-profile relationships in the atmosphere surface layer. *J. Atmos. Sci.*, **28**, 181-189.

Camillo, P. J. and R. J. Gurney, 1986: A resistance parameter for bare-soil evaporation models. *Soil Science*, **2**, 95-105.

Charney, J. G., W. J. Quirk, S. H. Chow, and J. Kornfield, 1977: A comparative study of the effects of albedo change on drought in semi-arid regions. *J. Atmos. Sci.*, **34**, 1366-1385.

Chen F., K. Mitchell, J. Schaake, Y. Xue, H.-l. Pan, V. Koren, Q. Duan, and A. Betts, 1995: Modeling of land-surface evaporation by four schemes and comparison with FIFE observations. Accepted by *J. Geophy. Res.*

Chen T. H. et al., 1995b: Cabauw experimental results from the project for intercomparison of land surface parameterization schemes. *J. Climate,* (In preparation).

Clapp, R. B. and G. M. and Hornberger, 1978: Empirical equations for some soil hydraulic properties. *Water Res. Res.*, **14**, 601-604.

Davies, R., 1982: Documentation of the solar radiation parameterization in the GLAS climate model. *NASA Tech. Memo.* 83961, 57 pp.

DeWitt, D. G., 1996: The effect of the cumulus convection scheme on the climate of the COLA general circulation model. *COLA Tech. Rep. 27,* 43 pp.

DeWitt, D. G. and E. K. Schneider, 1996: The Earth radiation budget as simulated by the COLA GCM. *J. Climate* (submitted).

Dorman, J. L., and P. J. Sellers, 1989: A global climatology of albedo, roughness length and stomatal resistance for atmospheric general circulation models as represented by the Simple Biosphere model (SiB). *J. Appl. Meteor.*, **28**, 833-855.

Eliassen, A. and E. Palm, 1961: On the transfer of energy in stationary mountain waves. *Geofys. Publ.*, **22**, 1-23.

European Centre for Medium Range Weather Forecasts Research Division, 1988: Research Manual 3: ECMWF Forecast Model Physical Parameterization. (ECMWF, Shinfield Park, U.K.).

Federer, C. A., 1979: A soil-plant-atmosphere model for transpiration and availability of soil water. *Water Res. Res.*, **153**, 555-562.

Fennessy, M. J., J. L. Kinter III, B. Kirtman, L. Marx, S. Nigam, E. Schneider, J. Shukla, D. Straus, A. Vernekar, Y. Xue, and J. Zhou, 1994: The simulated Indian monsoon: A GCM senstivity study. *J. Climate*, 7, 33-43.

Fennessy, M. J. and J. Shukla, 1996: Impact of initial soil wetness on seasonal atmospheric prediction. *COLA Tech. Rep. 34*, 25 pp.

Gardner, W. R. 1958: Some steady-state solutions of the unsaturated moisture flow equation with application to evaporation from a water table. *Soil Science,* **85**, 228-232.

Gibson, J. K., P. Kallberg, S. Uppala, A. Hernandez, A. Nomura, and E. Serrano, 1997: ERA description. *ECMWF Re-Analysis Proj. Rep. Ser. #1* (ECMWF, Shinfield Park, U.K.), 72 pp.

Haltiner, G. J. and R. T. Williams, 1980: Numerical Weather Prediction and Dynamic Meteorology, Second Edition (Wiley, New York), 477 pp.

Harshvardhan, R. Davis, D. A. Randall, and T. G. Corsetti, 1987: A fast radiation parameterization for general circulation models. *J. Geophys. Res.*, **92**, 1009-1016.

Harshvardhan, D. A. Randall, T. G. Corsetti, and D. A. Dazlich, 1989: Earth radiation budget and cloudiness simulations with a general circulation model. *J. Atmos. Sci.*, **46**, 1922-1942.

Helfand, H.M., J.C. Jusem, J. Pfaendtner, J. Tenenbaum and E. Kalnay, 1987: The effect of a gravity wave drag parameterization scheme in GLA fourth order GCM forecasts. (submitted to J. Appl. Sci.)

Hou, Y.-T., 1990: Cloud-Radiation-Dynamics Interaction. Ph.D. Thesis, University of Maryland, 209 pp.

Hurrell, J. W. and G. G. Campbell, 1992: monthly mean global satellite data sets available in CCM history tape format. *NCAR Tech. Note*, **NCAR/TN-371+STR**, 94 pp..

Jarvis, P. G., 1976: The interpretation of the variations in leaf water potential and stomatal conductance found in canopies in the field. *Philos. Trans. Roy. Soc. London*, **Ser. B.**, **273**, 593-610.

Kalnay, E., M. kanamitsu, R. Kistler, W. Collins, D. Deaven, L. Gandin, M. Iredell, S. Saha, G. White, J. Woollen, Y. Zhu, M. Chelliah, W. Ebisuzaki, W. Higgins, J. Janowiak, K. C. Mo, C. Ropelewski, J. Wang, A. Leetmaa, R. Reynolds, R. Jenne, D. Joseph, 1996: The NCEP/NCAR 40-year reanalysis project. *Bull. Amer. Meteor. Soc.*, 77, 437-471.

Kanamitsu, M., 1989: Description of the NMC global data assimilation and forecast system. *Wea. and Forecasting,* **4**, 225-342.

Kanamitsu, M., K. C. Mo, and E. Kalnay, 1990: Annual cycle integration of the NMC Medium Range Forecasting (MRF) model, *Mon. Wea. Rev.*, **118**, 2543-2567.

Kiehl, J. T., J. J. Hack, and B. P. Briegleb, 1994: The simulated Earth radiation budget of the National Center for Atmospheric Research community climate model CCM2 and comparisons with the Earth Radiation Budget Experiment (ERBE). *J. Geophys. Res.*, **99**, 20815-20827.

Killworth, Peter, 1996: Time interpolation of Forcing Fields in Ocean Models. *J. Phys. Ocean.*, **26**, 136-143.

Kinter III, J. L., J. Shukla, L. Marx and E. K. Schneider, 1988: A simulation of the winter and summer circulations with the NMC global spectral model. *J. Atmos. Sci.*, **45**, 2486-2522.

Kirtman, B. P., A. Vernekar, D. DeWitt, and J. Zhou, 1992: Impact of orographic gravity wave drag on extended range forecasts with the COLA GCM. *Atmosfera*, **6**, 3-24.

Kuo, H. L., 1965: On the formation and intensification of tropical cyclones through latent heat release by cumulus convection. *J. Atmos. Sci.*, **22**, 40-63.

Lacis A. and J. E. Hansen, 1974: A parameterization of the absorption of solar radiation in the Earth's atmosphere. *J. Atmos. Sci.*, **31**, 118-133.

Lindzen, R.S., 1981: Turbulence and stress due to gravity wave breakdown. *J. Geophys. Res.*, **87**, 3061-3080.

Liston, G. E., Y. C. Sud, and E. F. Wood, 1994: Evaluating GCM land surface hydrology parameterizations by computing river discharges using a runoff routing model: application to the Mississippi basin. *J. Appl. Meteor.*, **33**, 394-405.

Lord, S. J., W. C. Chao, and A. Arakawa, 1982: Interaction of a cumulus cloud ensemble with large- scale environment. Part IV: The discrete model. *J. Atmos. Sci.*, **39**, 104-113.

Louis, J.-F., 1979: A parametric model of vertical eddy fluxes in the atmosphere. *Bound.-Layer Meteorol.*, **17**, 187-202.

Machenauer, B., 1977: On the dynamics of gravity oscillations in a shallow water model with applications to normal mode initialization. *Beitr. Phys. Atmos.*, **50**, 253-271.

Manabe, S. 1969: The atmospheric circulation and hydrology of the Earth's surface. *Mon. Wea. Rev.*, **97**, 739-774.

Mellor, G. L. and T. Yamada, 1982: Development of a turbulence closure model geophysical fluid problems. *Rev. Geophys. Space Phys.*, **20**, 851-875.

Miyakoda, K. and J. Sirutis, 1977: Comparative integrations of global models with various parameterized processes of subgrid scale vertical transport: Description of the parameterizations. *Beitr. Phys. Atmos.*, **50**, 445-487.

Moorthi, S., and M. J. Suarez, 1992: Relaxed Arakawa-Schubert: A parameterization of moist convection for general circulation models. *Mon. Wea. Rev.*, **120**, 978-1002.

NMC Development Division Staff, 1988: Research version of the medium range forecast model. NMC Documentation Series #1 (available from the Development Division, NMC, Washington, D.C. 20233).

Orszag, S. A., 1970: Transform methods for calculation of vector coupled sums: Application to the spectral form of the vorticity equation. *J. Atmos. Sci.*, **27**, 890-895.

Paolino, D. P., Q. Yang, B. Doty, J. Kinter, J. Shukla, and D. M. Straus, 1994: Results of a pilot reanalysis project at COLA. *Bull. Amer. Meteor. Soc.*, **76**, 697-710.

Paulson, C. A., 1970: Mathematical representation of wind speed and temperature profiles in the unstable atmospheric surface layer. *J. Appl. Meteor.*, **9**, 857-861.

Peck, A. J., R. J. Luxmore, and J. L. Stolzy, 1977: Effects of spatial variability of soil hydraulic properties in water budget modeling. *Water Res. Res.*, **13**, 348-354.

Phillips, N. A., 1957: A coordinate system having some special advantages for numerical forecasting. *J. Meteor.*, **14**, 184-185.

Pierrehumbert, R. T. 1987: An essay on the parameterization of orographic gravity wave drag. Geophysical Fluid Dynamics Laboratory/NOAA, Princeton University, Princeton, NJ 08057.

Platzman, G. W., 1960: The spectral form of the vorticity equation. *J. Meteor.*, **17**, 635-644.

Posey, J. W. and P. F. Clapp, 1954: Global distribution of normal surface albedo. *Geofisica Int.*, **4**, 33-48.

Reynolds, R. W., 1982: A monthly averaged climatology of sea surface temperatures. NOAA Tech. Rept. **NWS 31**, Washington, DC. 33 pp.

Reynolds, R. W., 1988: A real-time global sea surface temperature analysis. *J. Climate*, **1**, 75-86.

Reynolds, R. W. and L. Roberts, 1987: A global sea surface temperature climatology from in situ, satellite and ice data. *Trop. Ocean-Atmos. Newslett.*, **37**, 15-17.

Reynolds, R. W. and T. M. Smith, 1995: A high resolution global sea surface temperature climatology. J. Climate, 8, 1571-1583.Robert, A. J., 1969: The integration of a spectral model of the atmosphere by the implicit method. **Proc. WMO/IUGG Symp. on Num. Wea. Prediction**, Tokyo, *Meteor. Soc. Japan*, VII-19-VII-24.

Robock, A., K. V. Vinnikov, V. A. Schlosser, N. A. Speranskaya, and Y. Xue, 1995: Use of Russian soil moisture and meteorological observations to validate soil moisture simulations with biosphere and bucket models. *J. Climate*, **8**, 15-35.

Sato, N., P. J. Sellers, D. A. Randall, E. K. Schneider, J. Shukla, J. L. Kinter III, Y.-T. Hou and E. Albertazzi, 1989a: Effects of implementing the Simple Biosphere Model in a general circulation model. *J. Atmos. Sci.*, **46**, 2757-2782.

Sato, N., P. J. Sellers, D. A. Randall, E. K. Schneider, J. Shukla, J. L. Kinter, III, Y.-T. Hou, and E. Albertazzi, 1989b: Implementing the simple biosphere model in a general circulation model: Methodologies and results. NASA Contractor Report 185509, 76 pp.

Schlosser, C. A., 1995: Land-surface hydrology: validation and intercomparison of multi-year off-line simulations using mid-latitude data. Ph.D. Dissertation, University of Maryland, College Park, Maryland, 132 pp.

Schneider, E. K. and J. L. Kinter III, 1994: An examination of internally generated variability in long climate simulations. *Climate Dyn.*, **10**, 181-204.

Schubert, S., R. Rood, and J. Pfaendtner, 1993: An assimilated data set for earth sciences applications. *Bull. Amer. Meteor. Soc.*, **74**, 2331-2342.

Sela, J. G., 1980: Spectral modeling at NMC. *Mon. Wea. Rev.*, **108**, 1279-1292.

Sellers, P. J., W. J. Shuttleworth, J. L. Dorman, A. Dalcher, and J. M. Roberts, 1989: Calibrating the single biosphere model for Amozonian tropical forest using feild and remote sensing data. Part I: Average calibration with field data. *J. Appl. Meteor.*, **28**, 727-759.

Sellers, P. J., Y. Mintz, Y. C. Sud, and A. Dalcher, 1986: A simple biosphere model (SiB) for use within general circulation models. *J. Atmos. Sci.*, **43**, 505-531.

Shao, Y. and A. Henderson-Sellers, 1995: Soil moisture simulation workshop review. Submitted to a special issue of *Global & Planetary Change*.

Shukla, J. and Y. Mintz, 1982: Influence of land surface evapotranspiration on the earth's climate. *Science*, **215**, 1498-1501.

Shukla, J. C. Nobre and P. J. Sellers, 1990: Amazon deforestation and climate change. *Science*, **247**, 1322-1325.

Slingo, J. M., 1987: The development of verification of a cloud prediction scheme for the ECMWF model. *Quart. J. Roy. Meteor. Soc.*, **13**, 899-927.

Smagorinsky, J., 1960: On the synamical prediction of large-scale condensation by numerical methods. *Phys. of Precipitation, Geophys. Monogr.*, Amer. Geophys. Union, **5**, 727-768.

Sud, Y. C. and W. E. Smith, 1985: The influence of surface roughness of deserts in the July circulation. *Bound. Layer Meteor.*, **33**, 15-40.

Sud, Y. and A. Molod, 1988: The roles of dry convection, cloud radiation feedback processes, and the influence of recent improvements in the parameterization of convection in the GLA GCM. *Mon. Wea. Rev.*, **116**, 2366-2387.

Tiedtke, M., 1983: The sensitivity of the time mean large scale flow to cumulus convection in the ECMWF model. *Workshop on Convection in Large Scale Numerical Models.* ECMWF, 297-316.

Trenberth, Kevin, 1992: Global Analysis for ECMWF and atlas of 1000 to 10 mb Circulation Statistics. *NCAR Technical Note-373+STR*, 191pp.

van Genuchten, 1980: A close-form equation for predicting the hydraulic conductivity of unsaturated soils. *Soil. Sci. Soc. Amer. J.*, **44**, 892-898.

Wetzel P. and J.-T. Chang, 1987: Concerning the relationship between evapotranspiration and soil moisture. *J. Climate Appl. Meteor.*, **26**, 18-27.

Willmott, C. J., C. M. Rowe and Y. Mintz, 1985: Climatology of the terrestrial seasonal water cycle. *Journal of Climatology*, **5**, 589-606.

Xue, Y., P. J. Sellers, J. L. Kinter III, and J. Shukla, 1991: A simplified biosphere model for global climate studies. *J. Climate*, **4**, 345-364.

Xue, Y., P. J. Sellers, J. L. Kinter III, and J. Shukla, 1991: A simplified biosphere model for global climate studies. *J. Climate*, **4**, 345-364.

Xue, Y. H. Bastable, P. Dirmeyer, and P. J. Sellers 1996: Sensitivity of simulates surface fluxes to changes in land surface parameterizations. *J. Appl. Meteor.*, **35**, 386-400.

**Figures**

Figure 1: Schematic diagram of the vertical arrangement of variables on discrete vertical levels. The left column gives the value of $\sigma$, the second column gives the level index, and the right column shows which variables are represented at a given level. The lowest vertical level is coincident with the Earth's surface ($\sigma = 1$). Prognostic variables are represented at levels shown with a dashed line, and the diagnostic vertical velocity is represented at levels shown with a solid line. The number of vertical levels resolved in the model corresponds to $K$ in this diagram.

Figure 2: Schematic diagram of SSiB. The transfer pathways for latent and sensible heat flux are shown on the left- and right-hand sides of the diagram, respectively. $T_r$ and $T_a$, and $e_r$ and $e_a$ are the air temperatures and specific humidity at reference height and within the canopy space, respectively; $T_c$ and $T_g$ are the canopy and the soil temperatures, respectively; $e*(T_c)$ and $e*(T_g)$ are the specific humidity at saturation at the canopy and the ground, respectively; $r_a$ the aerodynamic resistance between canopy air space and reference height; $r_b$ the bulk boundary layer resistance; $r_c$ the bulk stomatal resistance; $r_d$ aerodynamic resistance between canopy air space and ground; $r_{soil}$ the bare soil surface resistance. $H_c$ and $H_{gs}$ are the sensible heat flux from canopy and ground, respectively. $E_c$ and $E_s$ are the latent heat flux from canopy and ground, respectively. $f_h$ is the $\beta$ function to adjust bare soil evaporation.

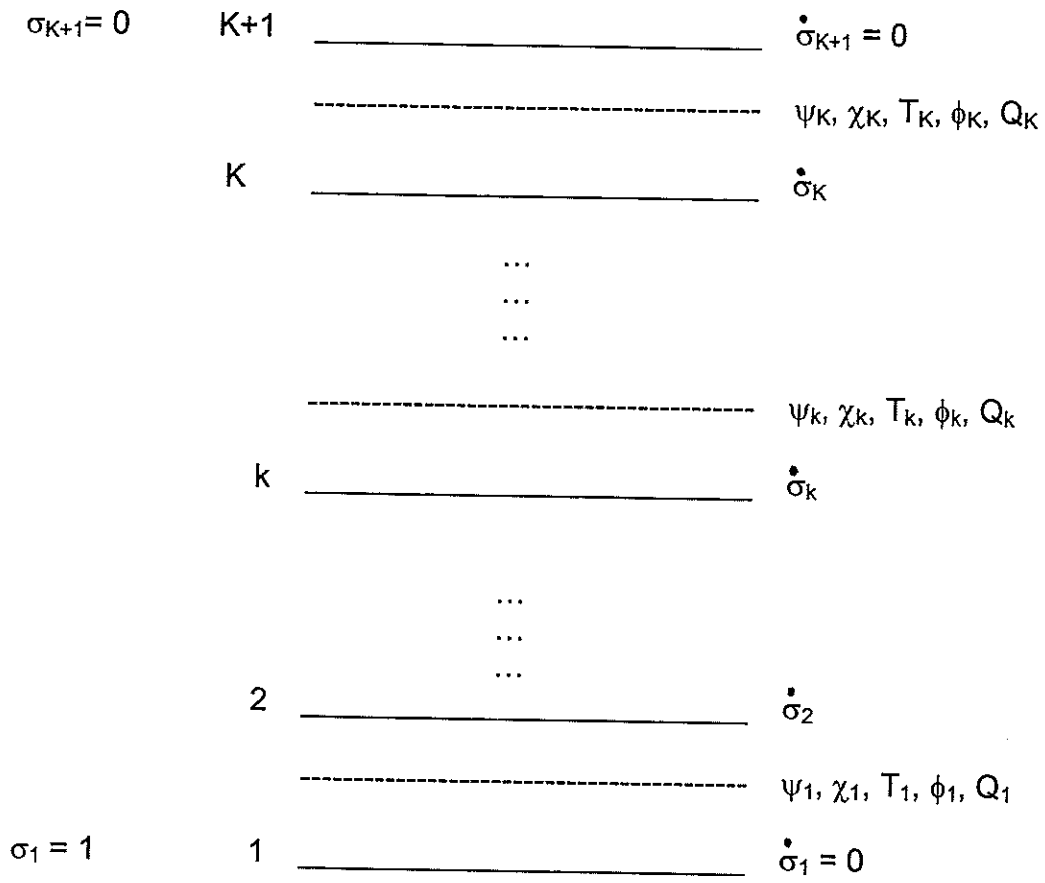
$\sigma_{K+1}= 0$
K+1
$\dot{\sigma}_{K+1} = 0$
$\psi_K, \chi_K, T_K, \phi_K, Q_K$
K
$\dot{\sigma}_K$
$\psi_k, \chi_k, T_k, \phi_k, Q_k$
k
$\dot{\sigma}_k$
2
$\dot{\sigma}_2$
$\psi_1, \chi_1, T_1, \phi_1, Q_1$
$\sigma_1 = 1$
1
$\dot{\sigma}_1 = 0$

**Figure 1**

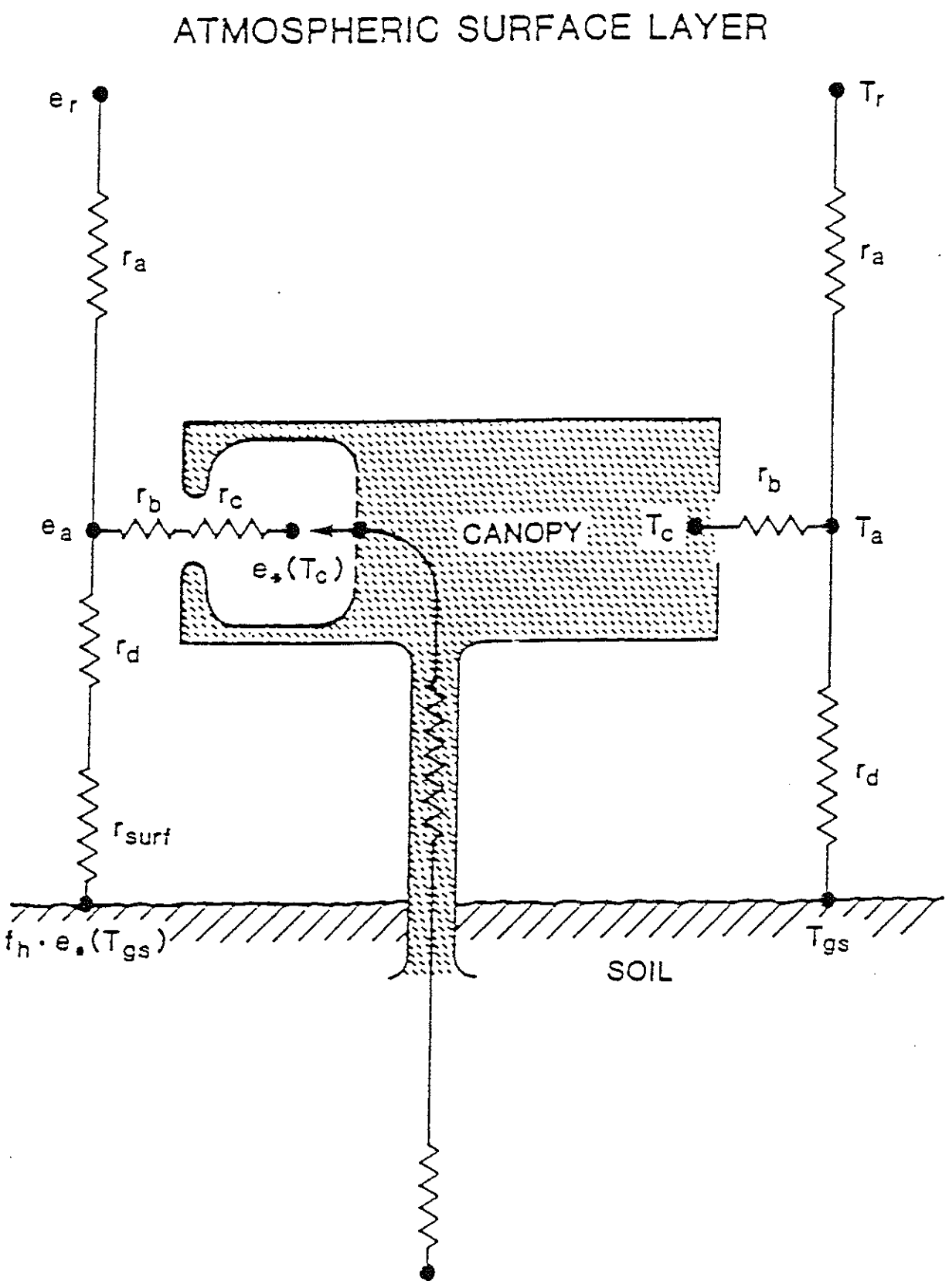
ATMOSPHERIC SURFACE LAYER
$e_r$
$T_r$
$r_a$
$r_a$
$r_b$
$r_c$
$r_b$
$e_a$
CANOPY
$T_c$
$T_a$
$e_*(T_c)$
$r_d$
$r_d$
$r_{surf}$
$f_h \cdot e_*(T_{gs})$
$T_{gs}$
SOIL

Figure 2